IEEE Access
Multidisciplinary | Rapid Review | Open Access Journal

Received 6 November 2023, accepted 20 November 2023, date of publication 28 November 2023,
date of current version 4 December 2023.

Digital Object Identifier 10.1109/ACCESS.2023.3336595

RESEARCH ARTICLE

Power Level Control of Nuclear Power Plants During Load Following Operation Using Fractional Order Controller Based on a Modified Algorithm

TAREK A. BOGHDADY[1], MOSTAFA MAHMOUD[1], ESSAM ABOUL ZAHAB[1], ELSAYED TAG-ELDIN[2], AND MAHMOUD SAYED[1]

[1]Department of Electrical Power Engineering, Faculty of Engineering, Cairo University, Giza, Cairo 12613, Egypt
[2]Faculty of Engineering and Technology, Future University in Egypt, New Cairo 11835, Egypt

Corresponding author: Mostafa Mahmoud (mostafa.mahmoud@eng.cu.edu.eg)

ABSTRACT Nuclear power can play an important role to achieve a secure clean energy transition. Output power control is considered an important issue with respect to nuclear power plants (NPPs) especially during load following operation mode. In this study, a scheduled fractional order proportional integral derivative (FOPID) controller is designed in order to track the desired reference power for a nuclear reactor in a NPP. Also, a modified manta ray foraging optimization (MMRFO) algorithm is proposed to tune the five parameters of the FOPID controller. The performance of the proposed algorithm is compared with several optimization techniques using 23 benchmark functions. The comparison shows that MMRFO has the best performance. The simulation of the FOPID controller tuned by the proposed MMRFO algorithm is performed using MATLAB/Simulink and its performance is compared with classic PID controller tuned by the MMRFO algorithm. Two different dynamic simulations during load following operation of a nuclear reactor are carried out. The first case study covers the short time operation of a nuclear reactor and the second case covers the long time operation. The simulation results show an acceptable performance with high degree of accuracy for the proposed FOPID controller tuned by the modified algorithm with very low overshoot, very low steady state error and proper control signal. Also, the stability of the proposed controller is also tested using Lyapunov stability criterion which indicates the stable operation for the proposed controller in the two cases. In addition, a sensitivity analysis has been accomplished which indicates the robustness of the controller.

INDEX TERMS Fractional order controller, manta ray foraging optimization, nuclear power plant, power level control, renewable energy resources.

NOMENCLATURE

P_0 = Rated output power (MW).
n_r = Neutron density relative to neutron density at full power.
c_{ri} = ith group normalized precursor density relative to density at full power.
X = Xenon concentration, cm^{-3}.
I = Iodine concentration, cm^{-3}.
λ_i = ith delayed neutron group decay constant, s^{-1}.
γ_x = Xenon yield per fission.
λ_x = Xenon decay constant, s^{-1}.
γ_I = Iodine yield per fission.
λ_I = Iodine decay constant, s^{-1}.
f_f = Fraction of reactor power deposited in fuel.
Σ_f = Macroscopic thermal neutron fission cross section.
V = Volume of the core, cm^3.
σ_X = Microscopic thermal neutron absorption cross section of xenon, cm^{-2}.
μ_f = Heat capacity of the fuel.
μ_c = Heat capacity of the coolant.
Ω = Heat transfer coefficient between fuel and coolant.

The associate editor coordinating the review of this manuscript and approving it for publication was Emanuele Crisostomi.

M = Mass flow rate times heat capacity of the coolant.
T_f = Average reactor fuel temperature (° C).
T_c = Temperature of the coolant (° C).
T_{co} = Temperature of the coolant at initial condition (° C).
α_f = Fuel temperature coefficient.
α_c = Coolant temperature coefficient.
T_{f0} = Average temperature of reactor fuel at initial condition.
T_{in} = Temperature of the entering coolant (° C).
T_{out} = Temperature of the leaving coolant (° C).
ρ = Reactivity (Δ k/k).
ρ_r = Reactivity due to control rod movement (Δ k/k).
z_r = Control rod speed in meter / sec..
G_r = Control rod total reactivity.
Λ = Neutron generation time.
β = Effective delayed neutron fraction.
β_i = ith group effective delayed neutron fraction.
λ = Effective precursor radioactive decay constant.
λ_i = ith delayed neutron group decay constant.
K_p = Proportional gain.
K_i = Integral gain.
K_d = Differential gain.
λ = Integral order.
μ = Differential order.
x_i^t = The position of the ith individual at time t in MRFO.
r = A random vector in the range of [0, 1].
γ = Weight coefficient of chain foraging in MRFO.
ω = Weight coefficient of cyclone foraging in MRFO.
It = The current iteration in MRFO.
$Itmax$ = The maximum number of iterations in MRFO.

I. INTRODUCTION

Global warming is one of the most severe problems that the world is facing nowadays which happens because of the generation of greenhouse gases like CO_2, methane and nitrous oxide. Although electric energy is clean at the point of usage, its generation leads to more than 40% of all energy-related carbon emissions. The Paris agreement targets to limit global warming to a value lower than 2 °C, nearly equal to 1.5 °C by 2050, compared to pre-industrial values [1].

Nuclear power has a great potential to contribute in Paris agreement goal since nuclear power plants (NPPs) generate no greenhouse gases during the operation period; only low emissions are generated through their life cycle. Beside the environmental reasons, the usage of nuclear energy can also decrease the imported fossil fuels [2].

According to the International Atomic Energy Agency (IAEA) reports, there are 442 nuclear power reactors in service in 32 countries. Also, there are 54 reactors under construction in 19 countries, with four countries that are building their first nuclear reactor [3]. The pressurized water reactor (PWR) is considered the most commonly utilized nuclear reactor in NPPs. NPPs were traditionally utilized in base load operation mode. Deep penetration of renewable energy sources – with its intermittent behavior - and increasing the percentage of nuclear energy in the electrical energy mix to meet the climate targets require studying and controlling the NPPs operation during load following operation to enable the power grid operator to generate and match different loads requirements. As an example, a daily energy demand cycle is shown in Figure 1. It is noted that nuclear power can provide flexible energy source in the presence of variable solar and wind generation without any need to fossil fuels based electrical energy. So, the operation of nuclear power reactors in load following operation mode must be studied and controlled. The main aim for a nuclear reactor control system is to determine insertion and withdrawal speed of reactor control rods while tracking the desired (reference) output power. The main target challenge is to obtain a smooth control signals with proper values from the controller to ensure safe operation for the actuators. Therefore, the main motivation of this study is to design an automatic controller (scheduled FOPID controller) to track the desired output power of a nuclear reactor during load following operation by determining the appropriate speed of reactor control rods. The main advantage of a scheduled FOPID controller over classic FOPID and PID controllers is that classic FOPID and PID controllers can deal with only one operating condition for the controlled system. On the other hand, the scheduled FOPID controller can deal with different operating conditions for the controlled system (different changes in the desired power for a PWR in this research).

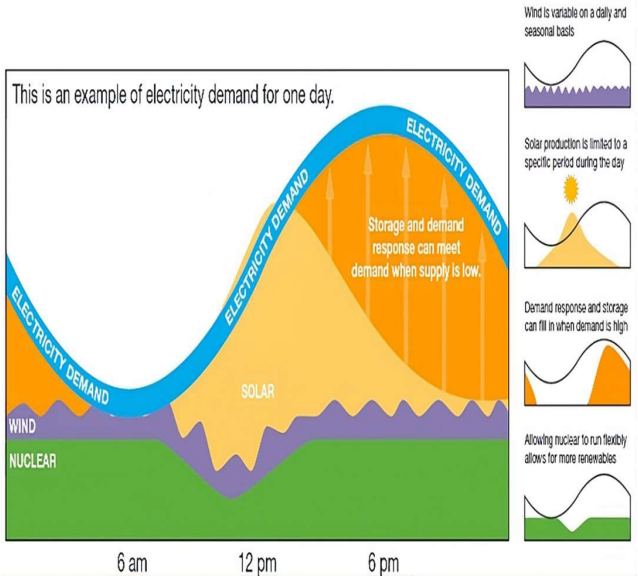

FIGURE 1. Daily energy demand cycle [3].

Different control strategies have been proposed to control the operation of nuclear reactors during load following mode. In [4] an adaptive proportional-differential controller

is presented to regulate the output power of a PWR. However, only one delayed neutron group is used to simulate the reactor model which is insufficient to describe the reactor dynamics. Also, L1-adaptive-based state-feedback control method is suggested using the linear quadratic Gaussian technique to achieve set-point optimal tracking without studying the stability of the controller and without monitoring both fuel and coolant temperatures [5]. An adaptive active fault-tolerant controller is designed for the load following operation of a modular high-temperature gas-cooled reactor (MHTGR) [6]. Unfortunately, only short time operation for the reactor is considered without performing stability analysis. A control strategy based on feed-forward compensation is proposed in [7] to improve the load following performance of the nuclear plant. A control scheme is designed for a PWR operation by integrating the optimal linear quadratic Gaussian control with the robust integral sliding mode controller in [8]. However, no sensitivity analysis is performed in [7] and [8]. Moreover, both fuel and coolant temperatures have not been monitoring during the load following operation of the reactor. An extended state observer-based sliding mode controller is presented for output power control of a PWR in a NPP with only one delayed neutron group for reactor modeling [9]. For the same purpose a fuzzy sliding mode controller is proposed in [10] without performing a stability analysis for the controller operation. A power control system based on power observer is developed in [11]. But, only long time operation for the reactor is studied. In [12], a chattering-free higher order sliding mode control scheme with a high-gain observer for the load following of a PWR is presented. However, only one delayed neutron group is used to model the reactor. A fractional order sliding mode control strategy via a disturbance observer is presented for load following operation of a MHTGR in [13]. Also, adaptive sliding mode control system is designed using point reactor kinetics equations for the load following of a NPP [14]. However, no sensitivity analysis is performed in [13] and [14]. A decentralized fuzzy model predictive control (DFMPC) is proposed in [15] where a fuzzy Lyapunov function and ''quasi-min-max'' strategy are utilized in designing the DFMPC without monitoring the control signal (control effort) produced by the controller. Monitoring the control signal is necessary to ensure safe operation for the actuators. Fuzzy based PID controller is proposed to control the output power of a nuclear reactor in short time operation in [16]. The usage of metaheuristic optimization techniques in the controller design has been proposed because of the ability of these algorithms in finding the optimum solution [17]. Different optimization techniques are used to determine the parameters of PID controllers [18] such as genetic algorithm in [19] and [20] for a 3000 MW PWR with point reactor kinetics model. Also, particle swarm optimization (PSO) is used in [21] and [22] to determine the controller parameters for a 3000 MW rated power PWR. The fractional order PID (FOPID) controller has been used in different published papers to control the output power of different types of nuclear reactors. The advantages of FOPID controllers compared to PID controllers include: lower steady-state error, less oscillations and overshoot, better response time, robustness to variations in parameters of the controlled system, and insensitivity to disturbing effects [23]. A fractional order PID controller is designed using genetic algorithm and the objective function was the integral of time-absolute error in [24]. Also, a FOPID controller tuned by genetic algorithm is presented in [25] to control the operation of advanced heavy water reactor. In [26] particle swarm optimization is used to tune FOPID parameters to control the output power of a nuclear reactor in short time operation. The output power is controlled in case of rapid reduction in reactor power using PSO based frequency domain tuning method for the FOPID controller [27].The Cuckoo Search optimization algorithm is also presented in order to tune the controller parameters during the load following operation of a molten salt reactor [28]. However, the optimization techniques used in these previous researches ([19], [20], [21], [22], [24], [25], [26], [27], and [28]) were selected without testing their performances. A fractional order controller is presented in [29] to control the output power of a pressurized heavy water reactor without any discussion to control signals values or coolant temperature changes. In [30], a fractional order controller is designed to control the operation of a PWR during load following operation. Only one delayed neutron group is considered in reactor modeling. Table 1 summarizes and compares this research with the previous researches.

The authors believe there is room to design a scheduled FOPID controller to control the output power of a PWR in a NPP in both short time operation and long time operation of the reactor. A Modified Manta Ray Foraging Optimization (MMRFO) algorithm is proposed to tune the parameters of the controller. The research's main contributions are:

1- Offering a scheduled FOPID controller to manage the operation of a PWR during load following operation instead of base load operation.
2- Offering a novel modified optimization algorithm named MMRFO to tune the parameters of the controller which is used to control the output power which is equivalent to the neutron density in the PWR. Before using the proposed algorithm, its performance is compared with different optimization techniques using 23 benchmark functions.
3- Discussing the performance of the controller in both short time operation and long time operation.
4- Monitoring fuel temperature, coolant temperature and control signals produced by the controller.
5- Studying the stability of the controller using Lyapunov stability criterion.
6- Providing a sensitivity analysis to validate the proposed controller.

This study is limited to a change in reactor desired power less than or equal to $\pm 5\%$ of reactor rated power per minute. Hard change in reactor desired power (when the set point power is changed with slope higher than $\pm 5\%$/minute) has

TABLE 1. Summary for the previous researches.

Controller	Tuning Technique
PD controller	Adaptive tuning [4]
L1 adaptive controller	Linear quadratic Gaussian technique [5]
Integral sliding mode controller	Optimal linear quadratic Gaussian technique [8]
Sliding mode controller	State observer feedback [9], high gain observer [11] and adaptive tuning [13]
Sliding mode controller	Fuzzy logic technique [10]
Model predictive controller	Fuzzy logic technique [15]
PID controller	Fuzzy logic [16], genetic algorithm [19-20] and particle swarm optimization [21-22]
FOPID controller	Genetic algorithm [24-25], particle swarm optimization [26-27] and cuckoo search optimization [28]
Scheduled FOPID controller	Modified manta ray foraging optimization (This research)

not been discussed in this paper. The authors recommend in the future to design a FOPID controller or any other nonlinear controller to control the reactor power in case of hard changes in the desired power. Also, taking into account the model of the steam turbine and model of the generator to subsequently control the output electrical power is taken as a future recommendation. The remainder of this paper is organized as follows: In Section III, the detailed model for the PWR is described. The proposed controller and the proposed modified algorithm are presented in Section IV. The tests and simulation results are included in Section V. Section VI present a sensitivity analysis for the proposed controller. Conclusions are drawn in the last section.

II. PWR MODEL DESCRIPTION

The first step for designing a control system for a reactor power is to select a reactor model. There are two types of mathematical models to simulate nuclear reactors dynamics. The first type is based on the distributed model resulting from partial differential equations and the second type obtained from ordinary differential equations which is named lump model. Although the distributed model is more accurate, the lumped model showed better overall performance in control system synthesis than distributed model. In this study, a 9th order nonlinear pressurized water reactor (PWR) model with three delayed neutron groups and reactivity feedbacks with xenon concentration, control rod movement, lumped coolant temperature and fuel temperature changes is used as in [20] and [31]. The neutron kinetics model with three groups of delayed neutron precursors is descripted in Eqs. (1) and (2). The atomic concentration of both xenon and iodine is descripted in Eqs. (3) and (4) [31].

$$\frac{dn_r}{dt} = \frac{\delta\rho - \beta}{\Lambda} n_r + \sum_{i=1}^{3} \frac{\beta_i}{\Lambda} c_{ri} \tag{1}$$

$$\frac{dc_{ri}}{dt} = \lambda_i n_r - \lambda_i c_{ri} \quad i = 1, 2, 3 \tag{2}$$

$$\frac{dX}{dt} = \frac{\left(\gamma_X \Sigma_f - \sigma_X X\right) P_0}{G \Sigma_f V} n_r - \lambda_X X + \lambda_I I \tag{3}$$

$$\frac{dI}{dt} = \frac{\gamma_I \Sigma_f P_0}{G \Sigma_f V} n_r - \lambda_I I \tag{4}$$

The PWR core must be cooled to eliminate the excess heat. The energy conservation for fuel and coolant must be investigated to describe the heat transfer as shown in Eqs. (5) and (6). Eq. (7) shows the control rod reactivity and Eq. (8) represents the total reactivity which results from xenon concentration, control rod movement, lumped coolant temperature and fuel temperature changes. The subscript (0) indicates the parameter value at nominal power [20].

$$\frac{dT_f}{dt} = \frac{f_f P_0}{\mu_f} n_r - \frac{\Omega}{\mu_f} T_f + \frac{\Omega}{2\mu_f} T_{in} + \frac{\Omega}{2\mu_f} T_{out} \tag{5}$$

$$\frac{dT_{out}}{dt} = \frac{\left(1 - f_f\right) P_0}{\mu_c} n_r + \frac{\Omega}{\mu_c} T_f - \frac{2M + \Omega}{2\mu_c} T_{out} + \frac{2M - \Omega}{2\mu_c} T_{in} \tag{6}$$

$$\frac{d\rho_r}{dt} = G_r z_r \tag{7}$$

$$\rho = \delta\rho_r + \alpha_f \left(T_f - T_{f0}\right) + \alpha_c \left(T_c - T_{c0}\right) - \frac{\sigma_X}{\Sigma_f}(X - X_0) \tag{8}$$

Moreover, as a function of initial equilibrium power n_{ro} the values of $\alpha_c, \alpha_f, \Omega, M$ *and* μ_c are as follows [32]:

$$\alpha_f\left(n_{ro}\right) = \left(n_{ro} - 4.24\right) \times 10^{-5} \tag{9}$$

$$\alpha_c\left(n_{ro}\right) = \left(-4n_{ro} - 17.3\right) \times 10^{-5} \tag{10}$$

$$\mu_c\left(n_{ro}\right) = \left(\frac{16}{9} n_{ro} + 54.022\right) \tag{11}$$

$$\Omega\left(n_{ro}\right) = \left(\frac{5}{3} n_{ro} + 4.9333\right) \tag{12}$$

$$M\left(n_{ro}\right) = \left(28 n_{ro} + 74\right) \tag{13}$$

The values of the PWR parameters are listed in Table 2 [32] in the middle of the fuel cycle at 100% of reactor rated power.

III. PROPOSED CONTROL STRATEGY

A. FOPID CONTROLLER

Fractional calculation has attracted great attention since it can give better control performance compared to classic PID controller due to the two added parameters which give more flexibility and better closed loop performance [33]. The fractional order approach converts a point-based control strategy to a modified plane-based strategy as shown in Figure 2 where the integer order controllers are represented as isolated points on the plane. The transfer function of the FOPID controller is as follows [20]:

$$G\left(s\right) = K_p + \frac{K_i}{s^{\lambda}} + K_d s^{\mu} \tag{14}$$

B. MANTA RAY FORAGING OPTIMIZATION (MRFO)

Manta Ray Foraging Optimization (MRFO) is a new meta-heuristic algorithm that simulates the foraging behaviors of

TABLE 2. PWR parameters.

Parameter	Value	Parameter	Value
P_o	2500 MW	λ	0.6813 (s^{-1})
Core height	400 cm	Σ_f	0.3358
Core radius	200 cm	σ_X/Σ_f	3.5×10^{-18} (Δk/k) cm^{-3}
f_f	0.91	β	0.0065
μ_f	26.3 (MW.s/°C)	Λ	0.00002 (s)
μ_c	71.8 (MW.s/°C)	λ_1	0.0124 (s^{-1})
Ω	6.6 (MW/°C)	λ_2	0.0369 (s^{-1})
M	102 (MW/°C)	λ_3	0.632 (s^{-1})
G_r	0.0145	β_1	0.00021
α_f	-0.0000324 (Δk/k.° C^{-1})	β_2	0.00225
α_c	-0.000213 (Δk/k.° C^{-1})	β_3	0.00404
γ_X	0.003	λ_X	2.1×10^{-5}
γ_I	0.059	λ_I	2.9×10^{-5}
G	3.2×10^{-11} MW.s	T_{in}	290°C

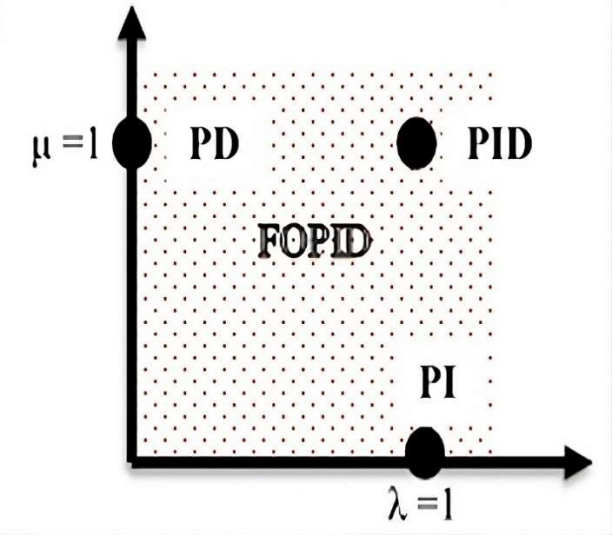

FIGURE 2. FOPID vs. PID controllers in a plane representation [23].

marine creatures called manta rays. Manta rays have three foraging strategies which are chain foraging, cyclone foraging and somersault foraging [34]. These foraging strategies are unique in nature which inspire this optimization technique.

1) CHAIN FORAGING

The manta rays arrange the foraging chain as a line via connecting their heads and tails. MRFO counts that the optimum solution has the higher concentration of plankton which is the desired food for manta rays. This represents the exploration of the algorithm. The mathematical model of chain foraging is as follows [35]:

$$x_i^{t+1} = \begin{cases} x_i^t + r * \left(x_{best}^t - x_i^t\right) + \gamma * \left(x_{best}^t - x_i^t\right), \\ \qquad i = 1 \\ x_i^t + r * \left(x_{i-1}^t - x_i^t\right) + \gamma * \left(x_{best}^t - x_i^t\right), \\ \qquad i = 2, 3, \ldots NP \end{cases} \tag{15}$$

$$\gamma = 2 * r * \sqrt{|\log(r)|} \tag{16}$$

2) CYCLONE FORAGING

When the concentration of plankton is very high, manta rays not only form long foraging chains and then move toward food but also move towards the food along a spiral path. This represents the exploitation of the algorithm. The mathematical model of cyclone foraging is as follows [36]:

$$x_i^{t+1} = \begin{cases} x_{best}^t + r * \left(x_{best}^t - x_i^t\right) + \omega * \left(x_{best}^t - x_i^t\right), \\ \qquad i = 1 \\ x_{best}^t + r * \left(x_{i-1}^t - x_i^t\right) + \omega * \left(x_{best}^t - x_i^t\right), \\ \qquad i = 2, 3, \ldots NP \end{cases} \tag{17}$$

$$\omega = 2 * \exp\left(r * \frac{Itmax - It + 1}{Itmax}\right) * \sin(2\pi r) \tag{18}$$

3) SOMERSAULT FORAGING

For this strategy, the food position is considered as a pivot location. Each individual turns around this pivot and then looks for the next position [37]. The mathematical model of somersault foraging is shown in Eq. (19) [37]:

$$x_i^{t+1} = x_i^t + S * \left(r_2 * x_{best}^t - r_3 * x_i^t\right), \quad i = 1, 2, ..NP \tag{19}$$

where S is the somersault factor.

C. MODIFIED MRFO (MMRFO)

1) MODIFIED CONTROL PARAMETER

MRFO manages the search process between chain foraging and cyclone foraging using a linearly increasing variable ($Coef$) which equals to ($It/Itmax$). This variable does not reflect the nonlinear search process. In this paper, a proposed S-Shaped control parameter is suggested as follows:

$$Coef = \sin^{2.5\cos\left(\frac{It}{Itmax}\right)^3}\left(0.5\pi\left(\frac{It}{Itmax}\right)\right) \tag{20}$$

The proposed S-Shaped strategy gives more probability for exploration in the first iterations to prevent the algorithm from

falling in local optimum. In last iterations, it gives higher probability for exploitation to accelerate the convergence. The difference between the linear control parameter in original MRFO and the proposed nonlinear control parameter is shown in Figure 3.

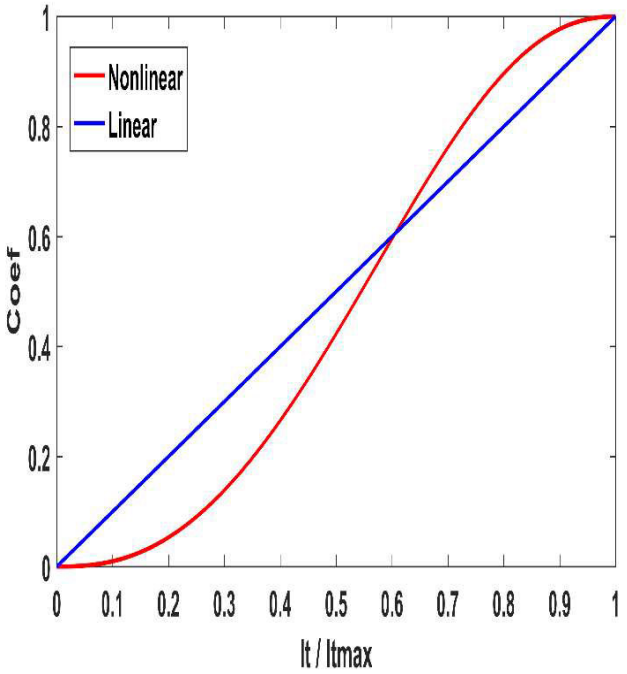

FIGURE 3. Linear vs. S-shaped control parameter.

2) MODIFIED SOMERSAULT PARAMETER

MRFO uses a constant value of somersault parameter ($S = 2$), but in the early iterations, the algorithm performs more exploratory behavior, so higher value for S is required to discover more space. In last iterations, the algorithm should give higher focus on exploitation, therefore, large value for S will weaken algorithm's exploitation ability. Therefore, a negative slope linear modified somersault parameter is suggested which equals to 2.2 at the first iteration and equals to 1.8 at the last iteration as follows

$$S = \frac{1.8 - 2.2}{Itmax} \times It + 2.2 \tag{21}$$

A flowchart for the proposed MMRFO algorithm is presented in Figure 4.

D. MMRFO TESTING

In order to examine the proposed MMRFO, its performance is compared with several recent optimization techniques such as Linearized Biogeography Based Optimization (LBBO) [38], Gray Wolf Optimization (GWO) [39], Whale Optimization Algorithm (WOA) [40] and Atom Search Optimization (ASO) [41] using 23 benchmark functions that were previously discussed and approved in the Congress of Evolutionary Computation (CEC) [42]. The definitions of these function are listed in Table 3 [42]. More details for these

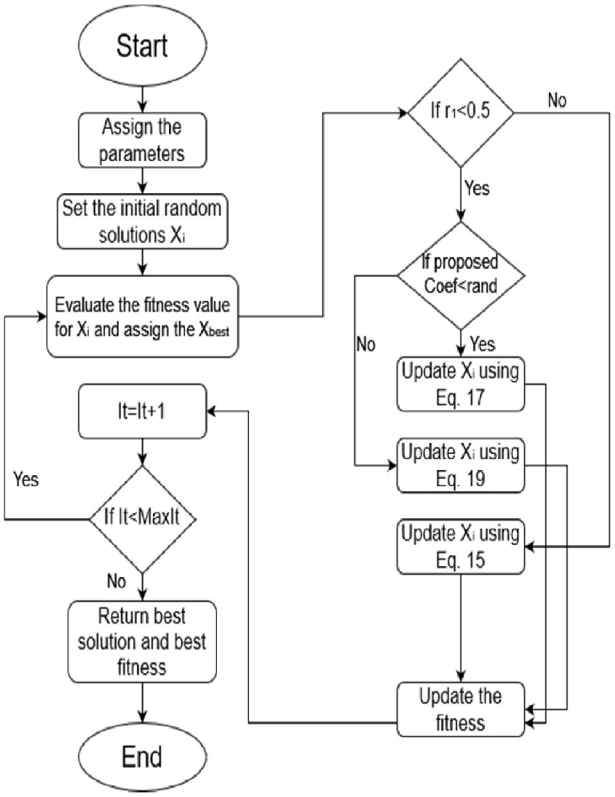

FIGURE 4. MMRFO flowchart.

functions including name, dimension, range and graphical representation can be found in [29] and [43]. To ensure fair comparison, the maximum number of iterations for each algorithm is set to be 300. The performance of each optimization technique is shown in Table 4. The number inside the rounded parentheses represents the algorithm rank for this function. The rank for each algorithm for a given benchmark function depends on how this algorithm returns a global optimum value near to the value determined by the CEC. The number next to the rounded parentheses represents the average value of the global optimum values obtained after 10 simulation runs. The last column indicates the global optimal value for this benchmark function that has been given by the CEC and the last row indicates the average rank for each algorithm over the 23 benchmark functions. It is noted that MMRFO has the best average rank.

E. MMRFO BASED CONTROLLER

The proposed MMRFO is used to determine the parameters of the scheduled FOPID controller and the parameters of a scheduled PID controller to compare the performances of both controllers. The maximum number of iterations is set to be 300 in order to obtain higher accuracy. The integral square error (ISE) is chosen to be the fitness (objective) function that will be minimized as follows:

$$ISE = \int_0^\infty e^2(t)\, dt \tag{22}$$

TABLE 3. Benchmark functions.

Index	Function
F1	$\sum_{i=1}^{n} x_i^2$
F2	$\sum_{i=1}^{n} \lvert x_i \rvert + \prod_{i=1}^{n} \lvert x_i \rvert$
F3	$\sum_{i=1}^{n} \left(\sum_{j=1}^{n} x_j\right)^2$
F4	$max_i\{\lvert x_i \rvert, 1 \le i \le n\}$
F5	$\sum_{i=1}^{n-1} \left(100\left(x_{i_{+1}} - x_i\right)^2\right) + (x_i - 1)^2$
F6	$\sum_{i=1}^{n} (x_i + 0.5)^2$
F7	$\sum_{i=1}^{n} i x_i^4 + random(0,1)$
F8	$-\sum_{i=1}^{n} (x_i \sin(\sqrt{\lvert x_i \rvert}))$
F9	$\sum_{i=1}^{n} (x_i^2 - 10\cos(2\pi x_i) + 10)^2$
F10	$-20\exp\left(-0.2\sqrt{\frac{1}{n}\sum_{i=1}^{n} x_i^2}\right) - \exp\left(\frac{1}{n}\sum_{i=1}^{n} \cos 2\pi x_i\right) + 20 + e$
F11	$\frac{1}{4000}\sum_{i=1}^{n} (x_i - 100)^2 - \prod_{i=1}^{n} \cos\left(\frac{x_i - 100}{\sqrt{i}}\right) + 1$
F12	$\frac{\pi}{n} 10 sin2(\pi y_1) + \sum_{i=1}^{n-1} (y_i - 1)^2 [1 + 10 sin2(\pi y_i + 1)] + (y_n - 1)^2 + \sum_{i=1}^{30} u(x_i, 10, 100, 4)$
F13	$0.1 sin2(3\pi x_1) + \sum_{i=1}^{29} (x_i - 1)^2 p[1 + sin2(3\pi x_{i+1})] + (x_n - 1)^2 [1 + sin2(2\pi x_{30})] + \sum_{i=1}^{30} u(x_i, 5, 10, 4)$
F14	$\frac{1}{\left(\frac{1}{500}\right) + \sum_{j=1}^{25} (1/(j + \sum_{i=1}^{2} (x_i + a_{ij})^6))}$
F15	$\sum_{i=1}^{11} \left\lvert a_i - \frac{x_1(b_i^2 + b_i x_2)}{b_i^2 + b_i x_3 + x_4} \right\rvert^2$
F16	$4x_1^2 - 2.1x_1^4 + \frac{1}{3}x_1^6 + x_1 x_2 - 4x_2^2 + 4x_2^4$
F17	$\left(x_2 - \frac{5.1}{4\pi^2}x_1^2 + \frac{5}{\pi}x_1 - 6\right)^2 + 10\left(1 - \frac{1}{8\pi}\right)\cos x_1 + 10$
F18	$[1 + (x_1 + x_2 + 1)^2 (19 - 14x_1 + 3x_1^2 - 14x_2 + 6x_1 x_2 + 3x_2^2)] * [30 + (2x_1 + 1 - 3x_2)^2 (18 - 32x_1 + 12x_1^2 + 48x_2 - 36x_1 x_2 + 27x_2^2)]$
F19	$-\sum_{i=1}^{4} \exp\left[-\sum_{j=1}^{3} a_{ij}\left(x_j - p_{ij}\right)^2\right]$
F20	$-\sum_{i=1}^{4} \exp\left[-\sum_{j=1}^{6} a_{ij}\left(x_j - p_{ij}\right)^2\right]$
F21	$-\sum_{i=1}^{5} \lvert (x_i - a_i)(x_i - a_i)^T + c_i \rvert^{-1}$
F22	$-\sum_{i=1}^{7} \lvert (x_i - a_i)(x_i - a_i)^T + c_i \rvert^{-1}$
F23	$-\sum_{i=1}^{10} \lvert (x_i - a_i)(x_i - a_i)^T + c_i \rvert^{-1}$

where $e(t)$ is the error signal. Figure 5 shows a block diagram for the proposed closed loop control strategy.

IV. TESTS, RESULTS AND DISCUSSION

In this section the performance of the proposed FOPID controller is tested and compared with a PID controller in case of short time operation and long time operation during the load following operation of the PWR. The simulation of the closed loop control system is performed using MATLAB software.

A. RESPONSE DUE TO SHORT TIME OPERATION

In this case (case 1) the reactor is delivering 80% of its rated power and the set point (desired response) power is increased to 90% of reactor rated power in 2 minutes (slope equals to +5%/min.) and then the set point is decreased to 82% of reactor rated power in 2 minutes (slope equals to −4%/min.). The operation of the PWR in this case is divided into four time periods. In each period, the parameters of the FOPID controller and the PID controller are optimized and

TABLE 4. Optimization techniques comparison.

	LBBO	GWO	WOA	ASO	MRFO	MMRFO	Optimum
F1	3.45e-19(4)	1.65e-14(6)	1.22e-45(3)	2.07e-16(5)	7.5e-264(2)	4.4e-271(1)	0
F2	6.45e-15(4)	5.62e-10(5)	5.88e-31(3)	1.28e-06(6)	8.4e-132(2)	1.1e-136(1)	0
F3	3e-11(3)	0.00181(4)	62086.7(6)	3422.9(5)	8.1e-258(1)	8.8e-258(2)	0
F4	2.94e-11(3)	0.000482(4)	42.45(6)	0.0197(5)	1.1e-129(2)	2.1e-131(1)	0
F5	0.389(1)	27.1875(4)	27.881(5)	29.396(6)	23.3969(2)	24.052(3)	0
F6	2.12(6)	0.49521(4)	1.667(5)	0(1)	0(1)	0(1)	0
F7	2.76e-02(5)	2.5e-03(3)	9.39e-03(4)	6.33e-02(6)	2.84e-04(2)	6.27e-05(1)	0
F8	-1.2e+03(6)	-7.1e+03(5)	-8.7e+03(2)	-7.2e+03(4)	-8.5e+03(3)	-9.2e+03(1)	-12.5e+03
F9	0(1)	5.11e-13(5)	0(1)	18.9(6)	0(1)	0(1)	0
F10	3.15e-04(5)	20.835(6)	1.5e-14(3)	7.75e-09(4)	8.88e-16(1)	8.88e-16(1)	8.88e-16
F11	3e-09(6)	6.88e-15(5)	0(1)	1.11e-16(4)	0(1)	0(1)	0
F12	3.98e-09(4)	4.83e-02(5)	9.34e-02(6)	3.52e-19(1)	6.69e-10(2)	2.99e-09(3)	0
F13	0.002(2)	0.7786(6)	0.4537(5)	0.0111(3)	0.1084(4)	5e-04(1)	0
F14	0.998(1)	0.998(1)	5.9288(6)	1.992(5)	0.998(1)	0.998(1)	0.998
F15	3.07e-04(1)	6.95e-04(5)	3.23e-04(3)	0.01(6)	3.07e-04(1)	4.24e-04(4)	3.075e-04
F16	-0.559(6)	-1.0316(1)	-1.0316(1)	-1.0316(1)	-1.0316(1)	-1.0316(1)	-1.03163
F17	0.3979(1)	5.3979(1)	0.3979(1)	0.3979(1)	0.3979(1)	0.3979(1)	0.398
F18	3(1)	3(1)	3(1)	3(1)	3(1)	3(1)	3
F19	3.7e-05(6)	-3.8628(1)	-3.855(5)	-3.8628(1)	-3.8628(1)	-3.8628(1)	-3.8628
F20	6.7e-08(6)	-3.322(1)	-3.3183(5)	-3.322(1)	-3.322(1)	-3.322(1)	-3.32
F21	0.0377(6)	-10.1496(3)	-5.054(5)	-10.1532(1)	-10.1532(1)	-10.1376(4)	-10.1532
F22	-5.87(4)	-10.4008(3)	-5.0895(5)	-10.4029(1)	-5.0877(6)	-10.4029(1)	-10.4029
F23	0.0784(6)	-10.5306(4)	-10.525(5)	-10.5364(1)	-10.5364(1)	-10.5364(1)	-10.5364
Average Rank	3.82608	3.60869	3.7826	3.26086	1.69565	**1.47826**	

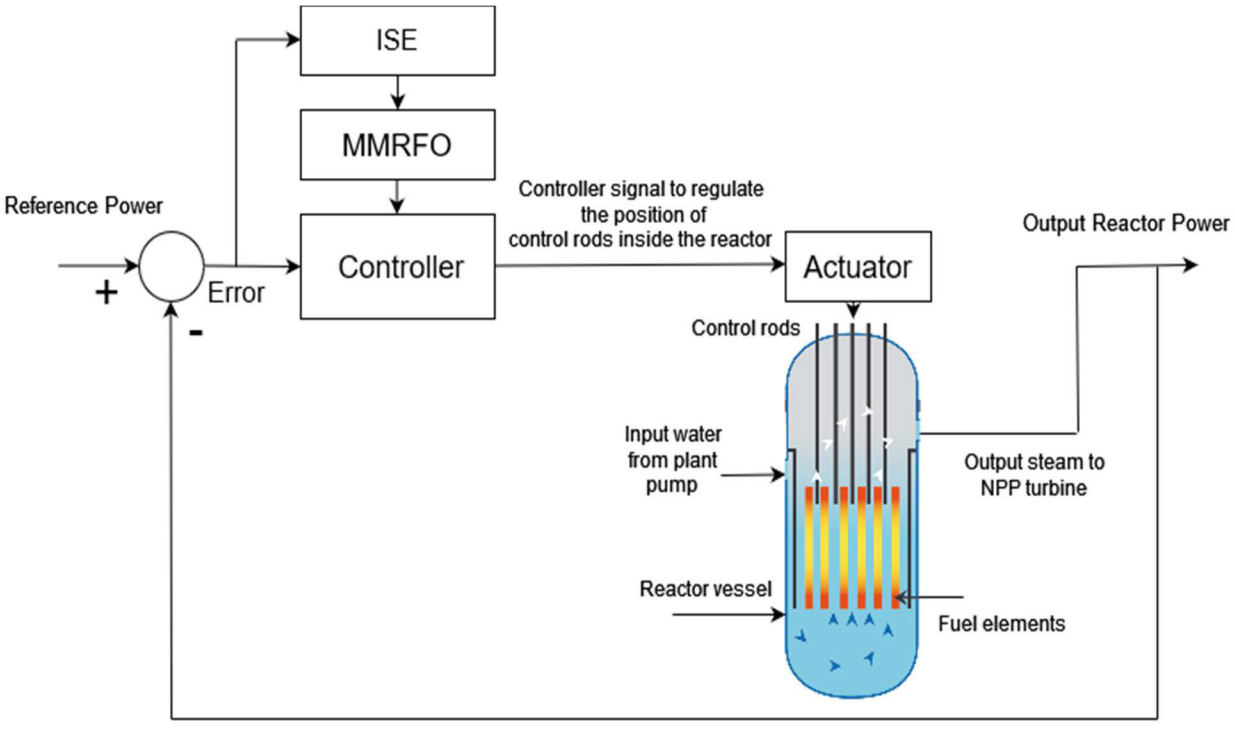

FIGURE 5. Diagram for the MMRFO based controller.

scheduled using the proposed MMRFO algorithm. Figures 6-7 show the convergence curves for the fitness function during the tuning of both controllers in each period. Figure 8 presents the relative output power in per-unit (PU) which is

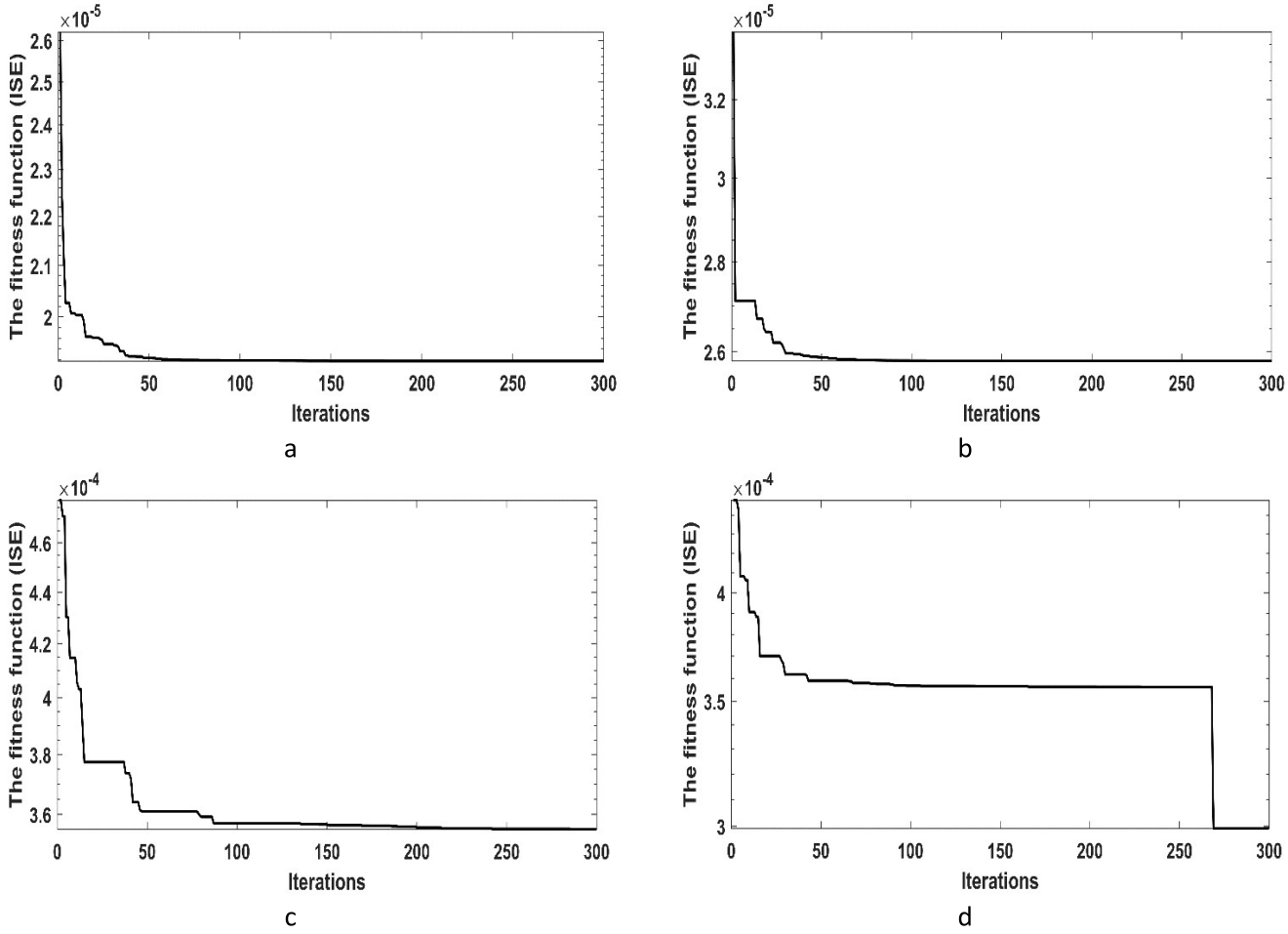

FIGURE 6. The change in fitness function for FOPID controller in case 1 at a)period 1, b)period 2, c)period 3 and d)period 4.

TABLE 5. Simulation results for the FOPID controller in case 1.

	Period 1	Period 2	Period 3	Period 4
Time limits (sec.)	0 - 420	420 - 550	550 - 660	660 - 800
K_p	29.676	32.193	28.761	24.845
K_i	6.766	3.334	2.769	4.241
K_d	8.419	4.032	4.289	5.002
λ	0.034	0.076	0.1	0.094
μ	0.201	0.3	0.265	0.093
Best fitness	1.9×10^{-5}	2.59×10^{-5}	3.58×10^{-4}	3×10^{-4}
Steady state error	3.9×10^{-5}	2.3×10^{-7}	1.1×10^{-7}	2.1×10^{-7}

equivalent to the relative neutron density. Simulation results and parameters of the scheduled FOPID and PID controllers are listed in Table 5 and Table 6.

It is noted from Figures 6, 7, 8, Table 5 and Table 6 that the scheduled FOPID controller has the best (least) fitness function value in each period. Also, the steady state error in case of the scheduled FOPID controller is lower than steady state error for the scheduled PID controller. Moreover, the FOPID-MMRFO controller has very fast response without overshoot. Therefore, the performance of the FOPID controller is better than performance of the PID controller. Figures 9-11 illustrate control rod speed, fuel temperature and coolant temperature resulting from applying the scheduled FOPID controller to the PWR. Table 7 lists the overshoot

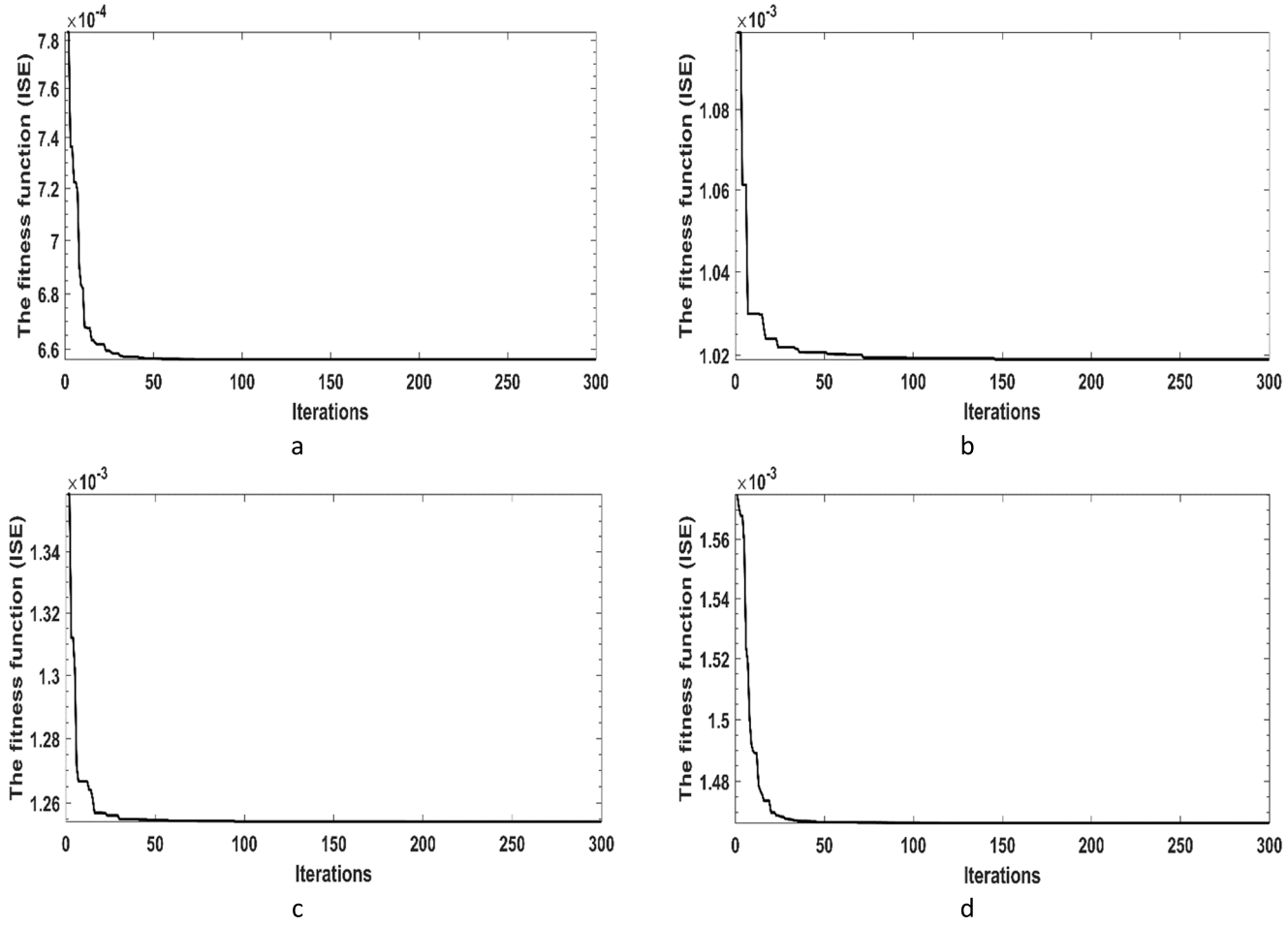

FIGURE 7. The change in fitness function for PID controller in case 1 at a)period 1, b)period 2, c)period 3 and d)period 4.

TABLE 6. Simulation results for the PID controller in case 1.

	Period 1	Period 2	Period 3	Period 4
Time limits (sec.)	0 - 420	420 - 550	550 - 660	660 - 800
K_p	21.826	22.163	17.752	14.885
K_i	5.546	3.106	3.129	5.541
K_d	5.589	3.982	7.319	5.611
Best fitness	6.58×10^{-4}	2.08×10^{-4}	1.254×10^{-3}	1.466×10^{-3}
Steady state error	2.4×10^{-3}	5×10^{-5}	2×10^{-7}	6.2×10^{-5}

and maximum control rod speed in each zone for the FOPID controller.

It is concluded from Figure 9 and Table 7 that the amplitude of the control rod speed (control effort) is accepted for the FOPID controller which means that there is no problem in the operation of the control actuators. Figures 10-11 illustrate that both fuel and coolant temperatures have the same trajectory as the reactor output power.

B. RESPONSE DUE TO LONG TIME OPERATION

In this case (case 2) the reactor is delivering 80% of its rated power and the set point power is increased to 90% of reactor rated power in 10 minutes (slope equals to +1%/min.) and then the set point is decreased to 82% of reactor rated power in 10 minutes (slope equals to −0.8%/min.). The operation of the PWR in this case is divided into four time periods. Like the previous case, the parameters of the FOPID controller

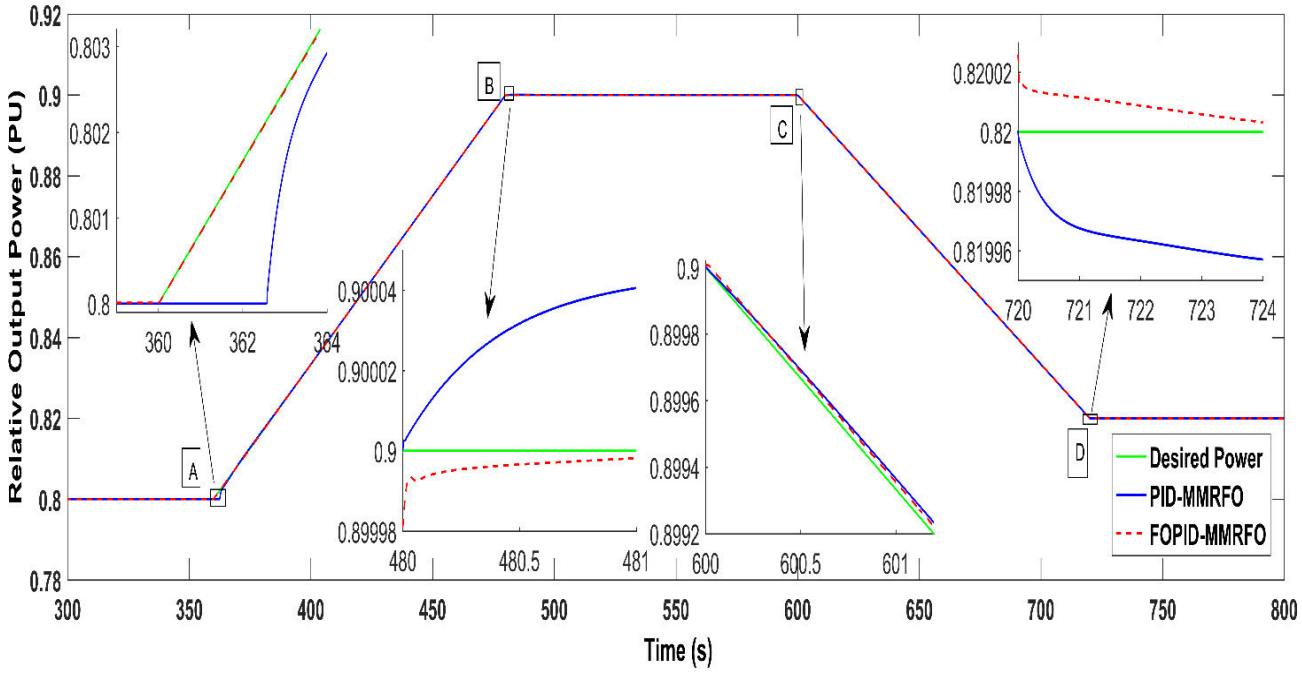

FIGURE 8. Relative output power in case one.

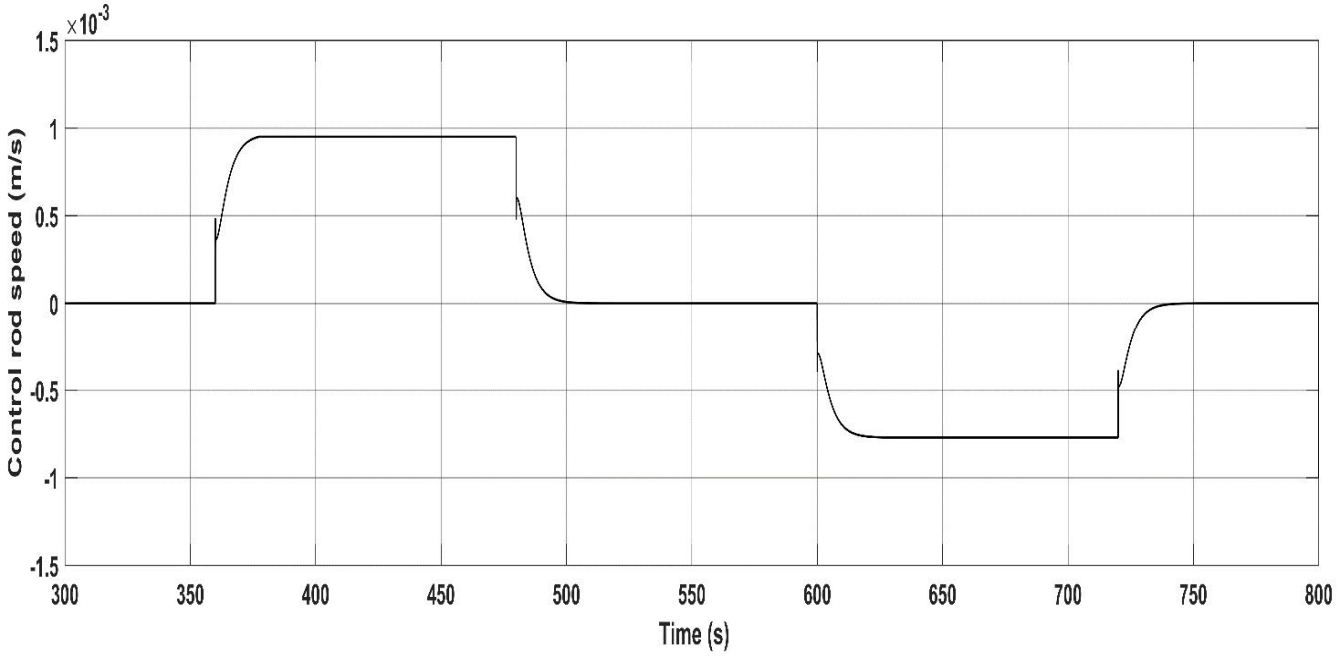

FIGURE 9. Control rod speed for the FOPID controller in case one.

and the PID controller are optimized and scheduled using the proposed MMRFO algorithm. Figures 12-13 show the convergence curves for the fitness function during the tuning of both controllers in each period. Figure 14 illustrates the relative output power in this case. Simulation results and parameters of the scheduled FOPID and PID controllers are listed in Table 8 and Table 9.

It is noted from Figures 12, 13, 14, Table 8 and Table 9 that the scheduled FOPID controller has least (best) fitness function value in each period with the

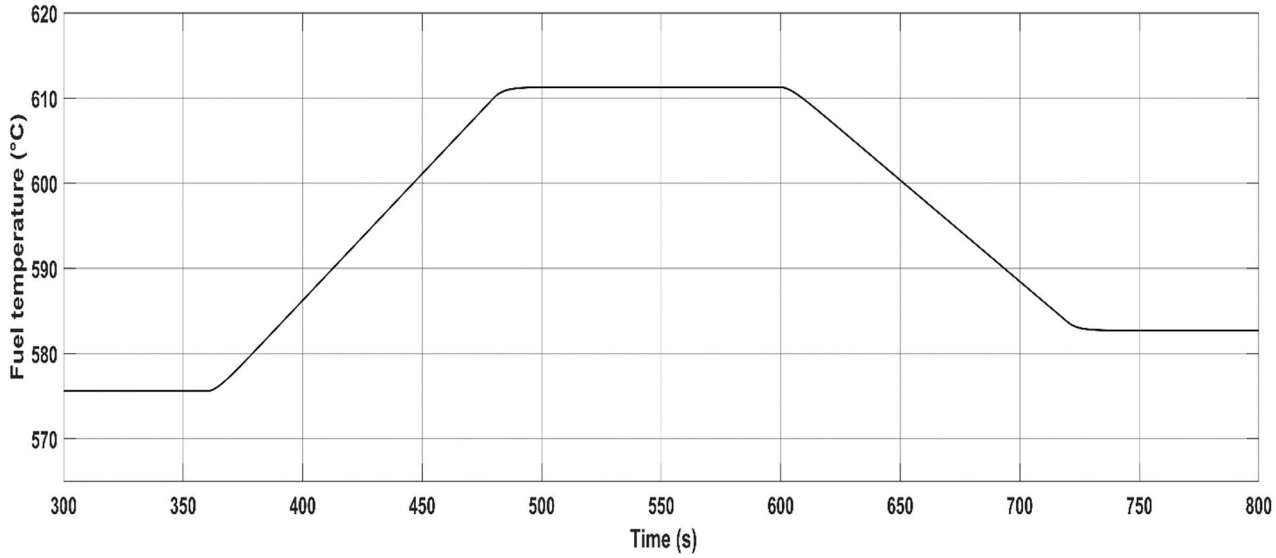

FIGURE 10. Fuel temperature for the FOPID controller in case one.

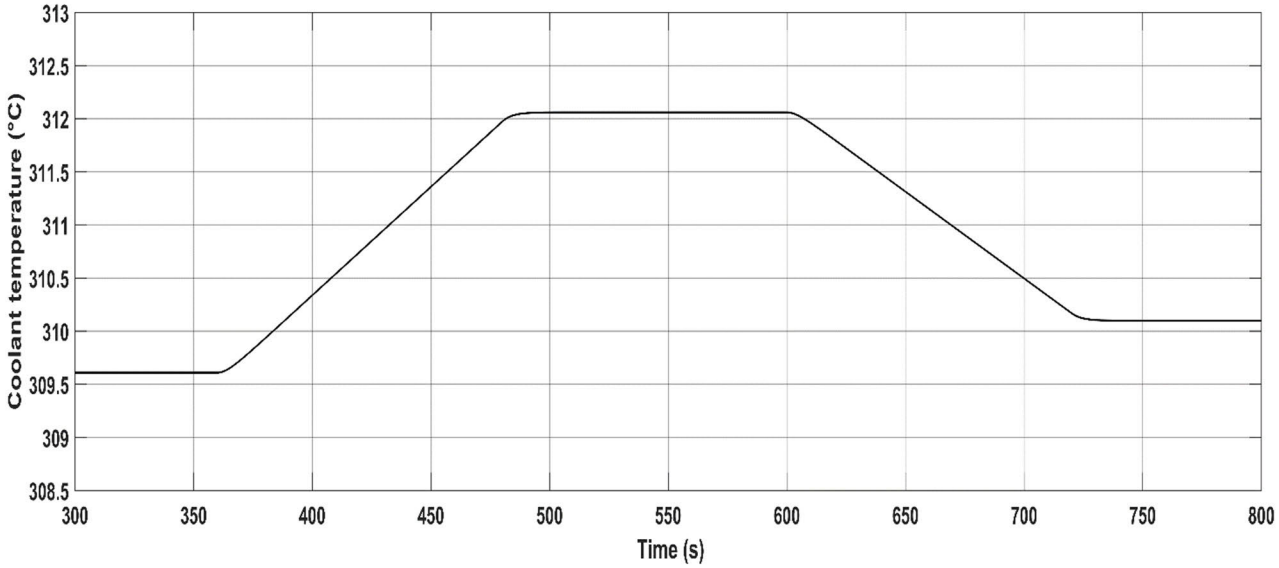

FIGURE 11. Coolant temperature for the FOPID controller in case one.

TABLE 7. Overshoot/undershoot and max. control rod speed for the FOPID controller in case 1.

	Period 1	Period 2	Period 3	Period 4
Time limits (sec.)	0 - 420	420 - 550	550 - 660	660 - 800
Overshoot/ undershoot	2.1×10^{-6}	1.11×10^{-3}	1.38×10^{-3}	7.31×10^{-3}
Max. control rod speed	0.095 cm/sec.	0.095 cm/sec.	0.078 cm/sec.	0.078 cm/sec.

minimum steady state error. Figures 15-17 present control rod speed, fuel temperature and coolant temperature resulting from applying the scheduled FOPID controller to the PWR. Table 10 presents the overshoot and

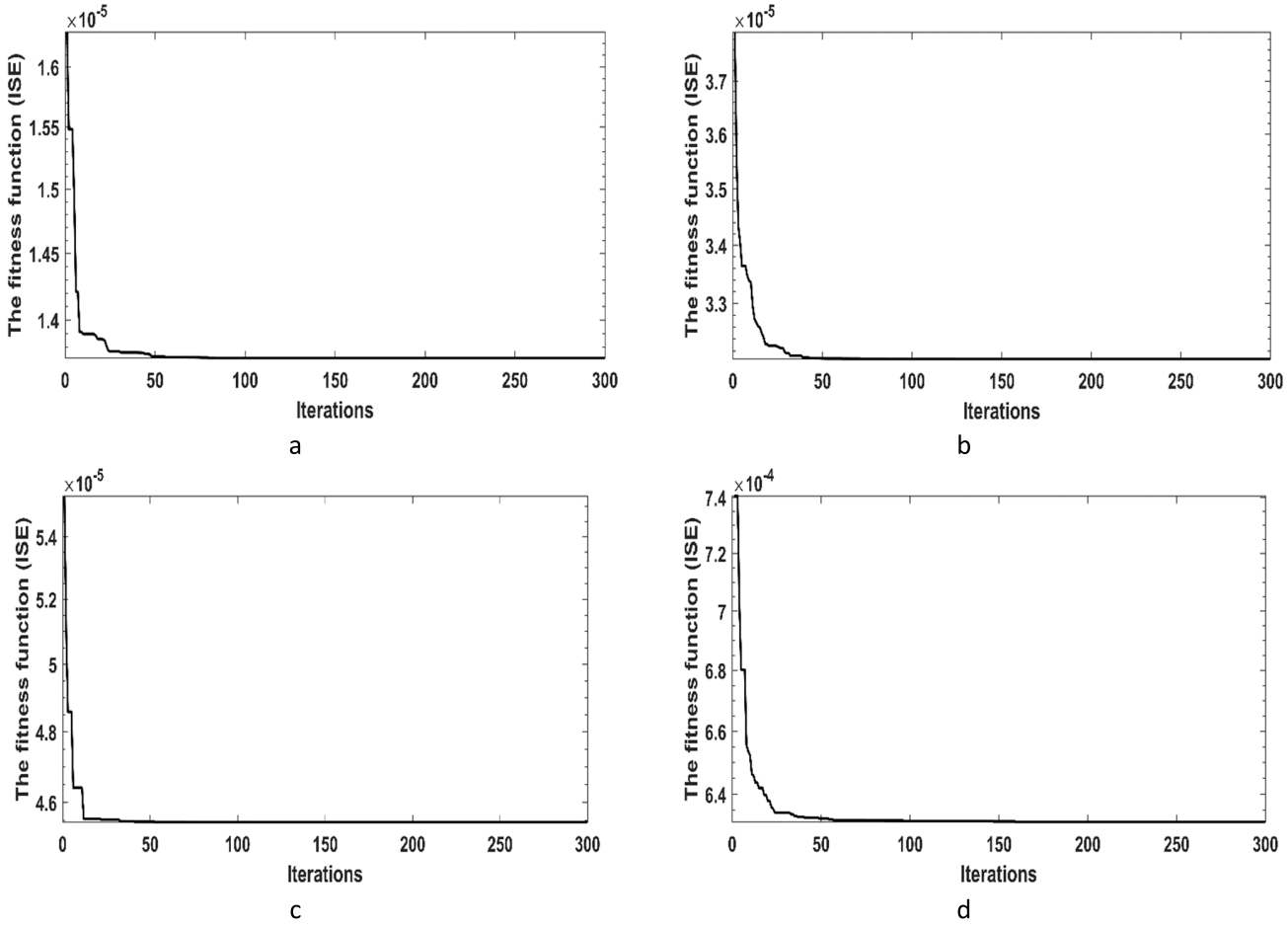

FIGURE 12. The change in fitness function for FOPID controller in case 2 at a)period 1, b)period 2, c)period 3 and d)period 4.

TABLE 8. Simulation results for the FOPID controller in case 2.

	Period 1	Period 2	Period 3	Period 4
Time limits (sec.)	0 - 600	600 - 1100	1100 - 1550	1550 - 1950
K_p	17.816	11.155	9.861	8.831
K_i	26.791	31.81	29.717	34.087
K_d	18.879	41.652	24.2	19.433
λ	0.039	0.09	0.05	0.01
μ	0.229	0.41	0.155	0.17
Best fitness	1.37×10^{-5}	3.2×10^{-5}	4.56×10^{-5}	6.36×10^{-4}
Steady state error	8.2×10^{-5}	1.2×10^{-6}	3.3×10^{-5}	7×10^{-5}

maximum control rod speed in each period for the FOPID controller.

Figure 14 indicates that the FOPID-MMRFO controller has very high tracking capability while tracking the desired output power. It can be concluded from Figure 15 and Table 10 that the control rod speed (control effort) has also accepted values during the load following operation of the PWR in this case. Both fuel and coolant temperatures have the same trajectories like the reactor power level as shown in Figure 16 and Figure 17.

In general, the proposed FOPID controller showed up high accuracy in tracking the desired output power in both short and long duration operation since for the short time operation the highest (worst) fitness function value is 3.58 × 10-4

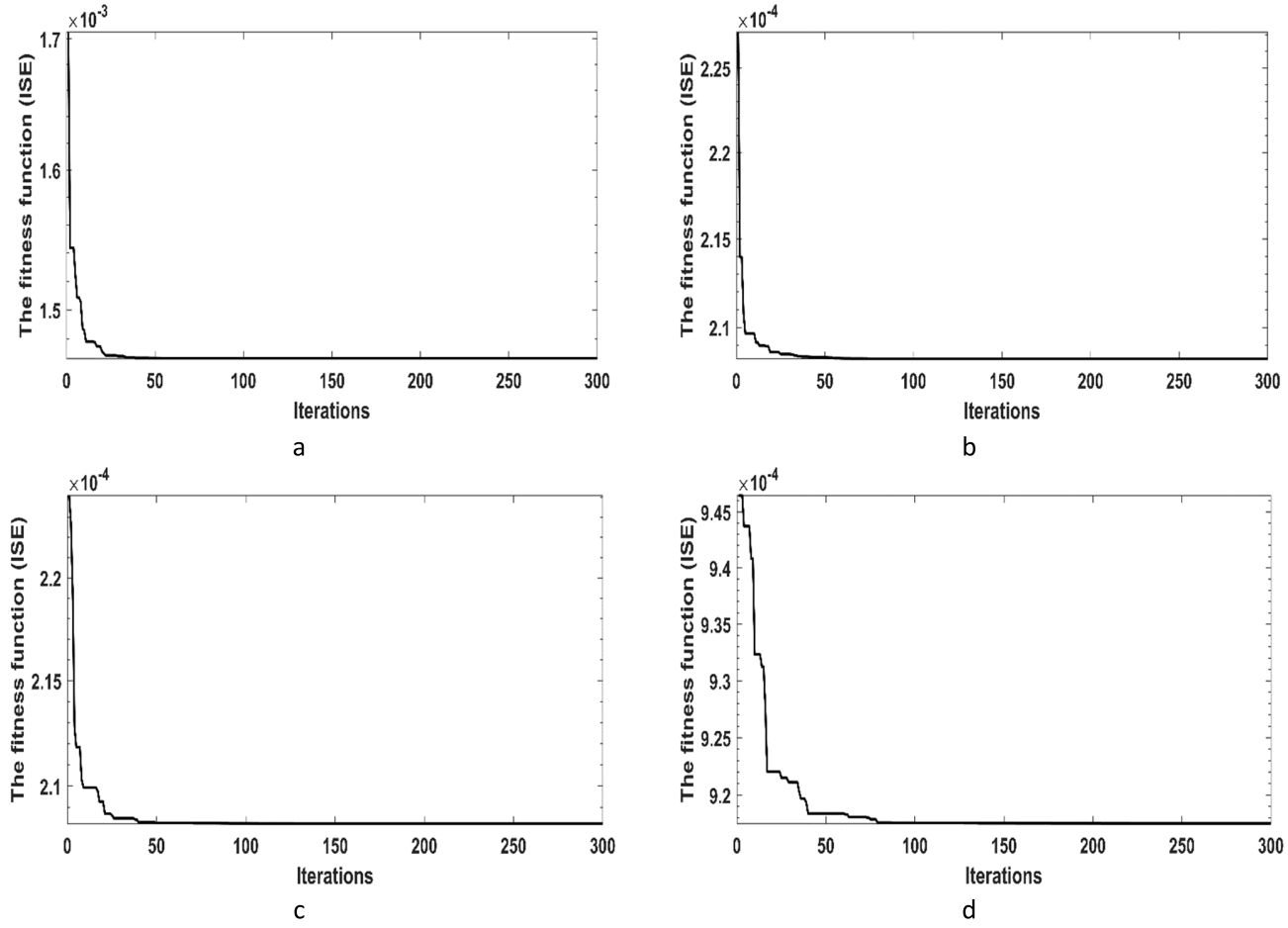

FIGURE 13. The change in fitness function for PID controller in case 2 at a)period 1, b)period 2, c)period 3 and d)period 4.

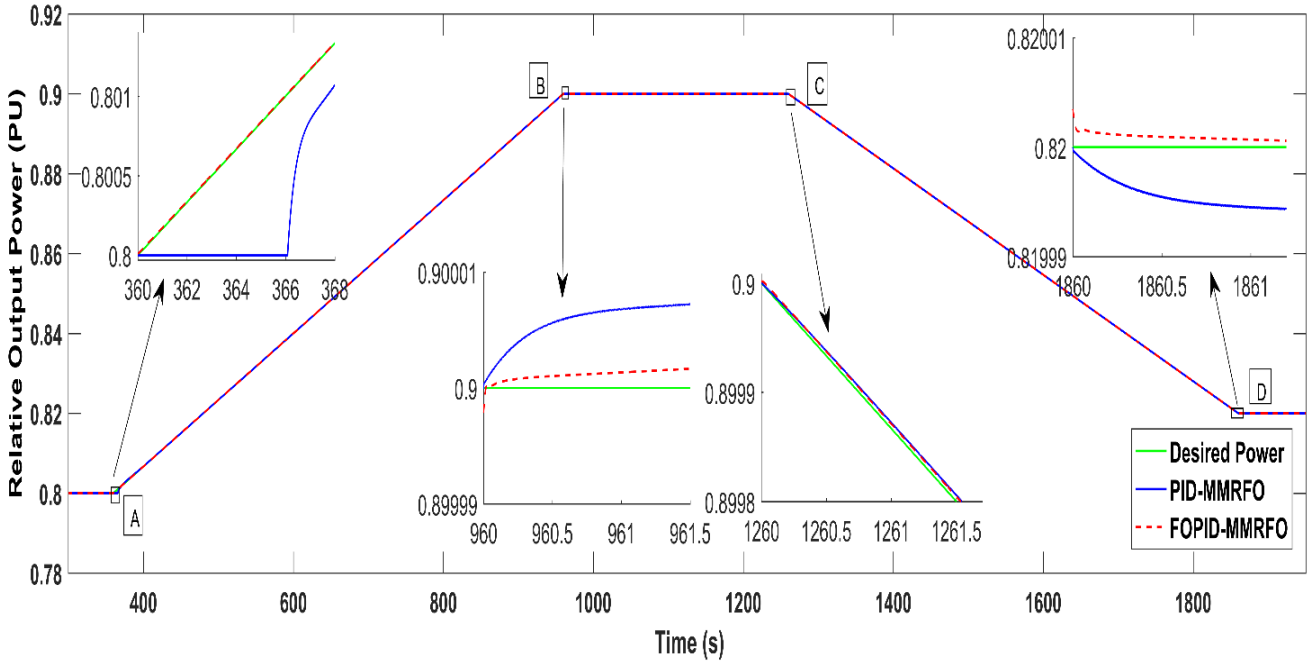

FIGURE 14. Relative output power in case two.

TABLE 9. Simulation results for the PID controller in case 2.

	Period 1	Period 2	Period 3	Period 4
Time limits (sec.)	0 - 600	600 - 1100	1100 - 1550	1550 - 1950
K_p	15.116	10.177	10.596	8.015
K_i	24.731	28.367	26.761	22.541
K_d	14.399	31.932	21.219	11.721
Best fitness	2.08×10^{-4}	1.56×10^{-3}	9.152×10^{-4}	1.02×10^{-3}
Steady state error	4.3×10^{-3}	6.2×10^{-5}	2.4×10^{-5}	4.2×10^{-3}

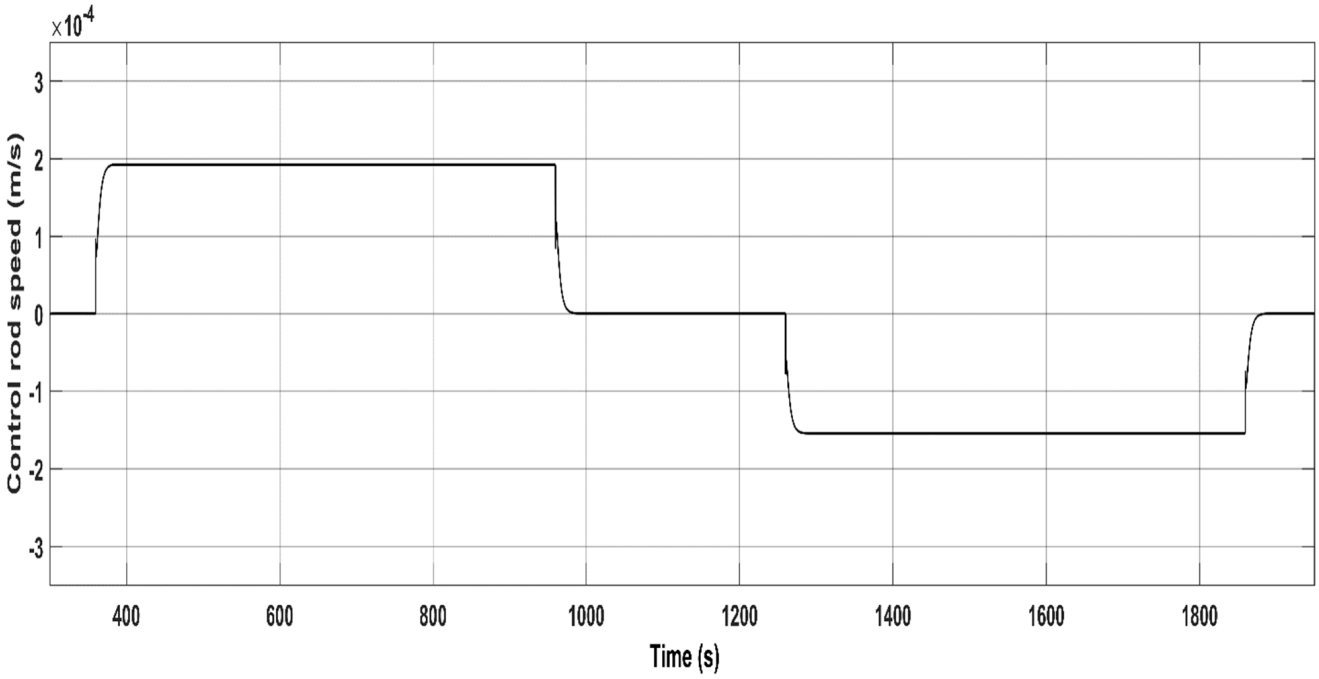

FIGURE 15. Control rod speed for the FOPID controller in case two.

TABLE 10. Overshoot/undershoot and max. control rod speed for the FOPID controller in case 2.

	Period 1	Period 2	Period 3	Period 4
Time limits (sec.)	0 - 600	600 - 1100	1100 - 1550	1550 - 1950
Overshoot/ undershoot	1.25×10^{-3}	7.11×10^{-6}	1.3×10^{-3}	1.13×10^{-3}
Max. control rod speed	0.019 cm/sec.	0.019 cm/sec.	0.0155 cm/sec.	0.0155 cm/sec.

in zone (C). Also, the maximum overshoot (worst value) is 7.31 × 10-3%, maximum steady state error is 3.9 × 10-5 and maximum control rod speed 0.095 cm/sec. For the long time operation the highest (worst) fitness function value is 6.36 × 10-4 in zone (D). Also, the maximum overshoot (worst value) is 1.3 × 10-3%, maximum steady state error is 8.2 × 10-5 and maximum control rod speed 0.019 cm/sec. Moreover, the coolant temperature is varying from 309.6°C to 312.05°C in

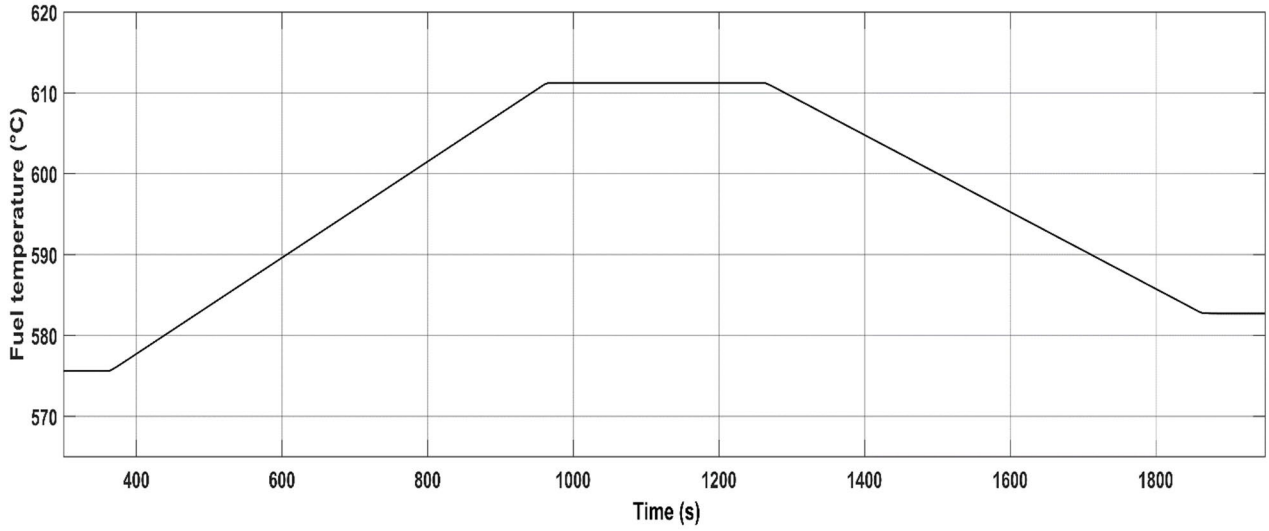

FIGURE 16. Fuel temperature for the FOPID controller in case two.

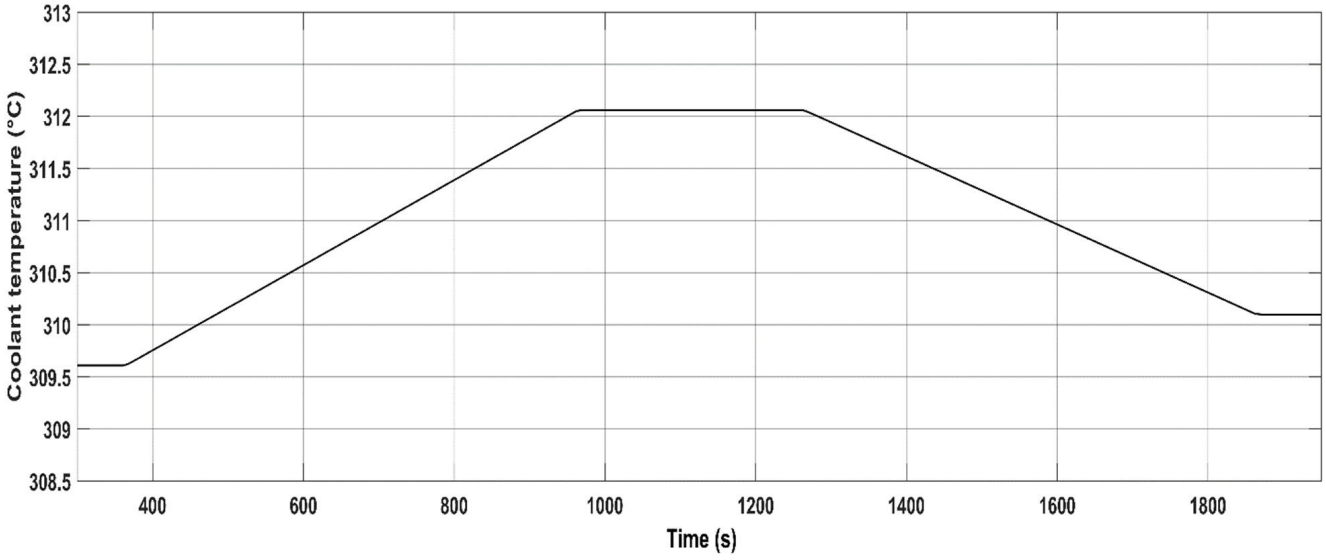

FIGURE 17. Coolant temperature for the FOPID controller in case two.

both cases and the fuel temperature is varying from 576°C to 612°C and the variation trajectory is similar to the reactor output power trajectory.

C. STABILITY ANALYSIS

In this section, a stability analysis for the performance of the proposed FOPID-MMRFO controller is performed using Lyapunov stability criterion. The Lyapunov function is defined as follows [44]:

$$\mathrm{V} = \frac{1}{2}\mathrm{e}^2 \tag{23}$$

where V : The Lyapunov function and e : The tracking error

The Lyapunov stability criterion states that when the derivative of Lyapunov function is lower than or equal to zero, then the stability condition is satisfied [44] as follows:

$$\dot{V} = \mathrm{e}.\dot{\mathrm{e}} \leq 0 \tag{24}$$

where

$\dot{V}$: The derivative of Lyapunov function (Lyapunov stability criterion)

$\dot{e}$: The derivative of the tracking error

Figure 18 and Figure 19 present the change of the derivative of Lyapunov function with time in zone A, zone B, zone C and zone D which are the transition periods shown in Figure 8

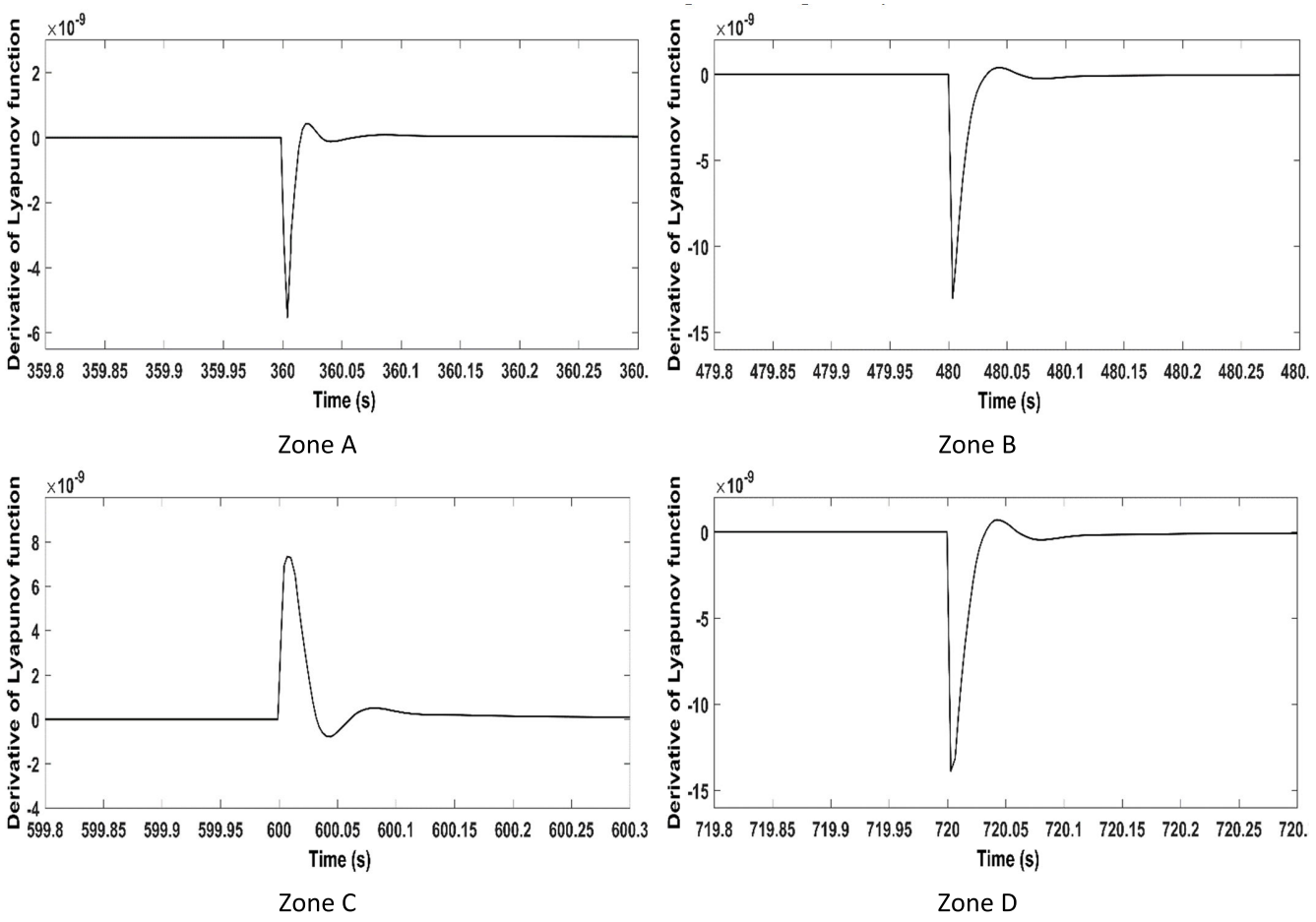

FIGURE 18. The derivative of the Lyapunov function with time for the FOPID controller in short time operation (case 1).

TABLE 11. Stabilization time in each case.

Case Number	Stabilization Time
Case 1(zone A)	0.2 sec.
Case 1(zone B)	0.15 sec.
Case 1(zone C)	0.3 sec.
Case 1(zone D)	0.15 sec.
Case 2(zone A)	0.2 sec.
Case 2(zone B)	0.1 sec.
Case 2(zone C)	0.25 sec.
Case 2(zone D)	0.15 sec.

and Figure 14 for both short time operation and long time operation respectively.

It is noted that stability condition is well satisfied in all zones according to the Lyapunov stability analysis and the stabilization is established in a short time according to Eq. (24) and maintained until the end of each zone in case 1 and case 2 as shown in Table 11 which lists the stabilization time in seconds in each zone for the two cases. Table 11 illustrates that the stabilization time does not exceed 0.3 seconds in any zone. Therefore, the operation of the proposed FOPID-MMRFO controller is stable in both short and long duration operation.

V. SENSITIVITY ANALYSIS

In order to validate the proposed FOPID-MMRFO controller and to check its robustness, a sensitivity analysis is performed. The delayed neutron effective fractions (β), coolant temperature coefficient (α_c) and fuel temperature coefficient (α_f) are reduced by 5% from their nominal values to conduct the sensitivity analysis and the relative output power, coolant temperature and fuel temperature are monitored in case one and case two.

It is noted that from figures 20-23 that the relative output power in both cases is well controlled like the two base cases. Also, the robustness of the controller is shown in the variation behavior of both fuel temperature in Figures 21-24 and coolant temperature as presented in Figures 22-25.

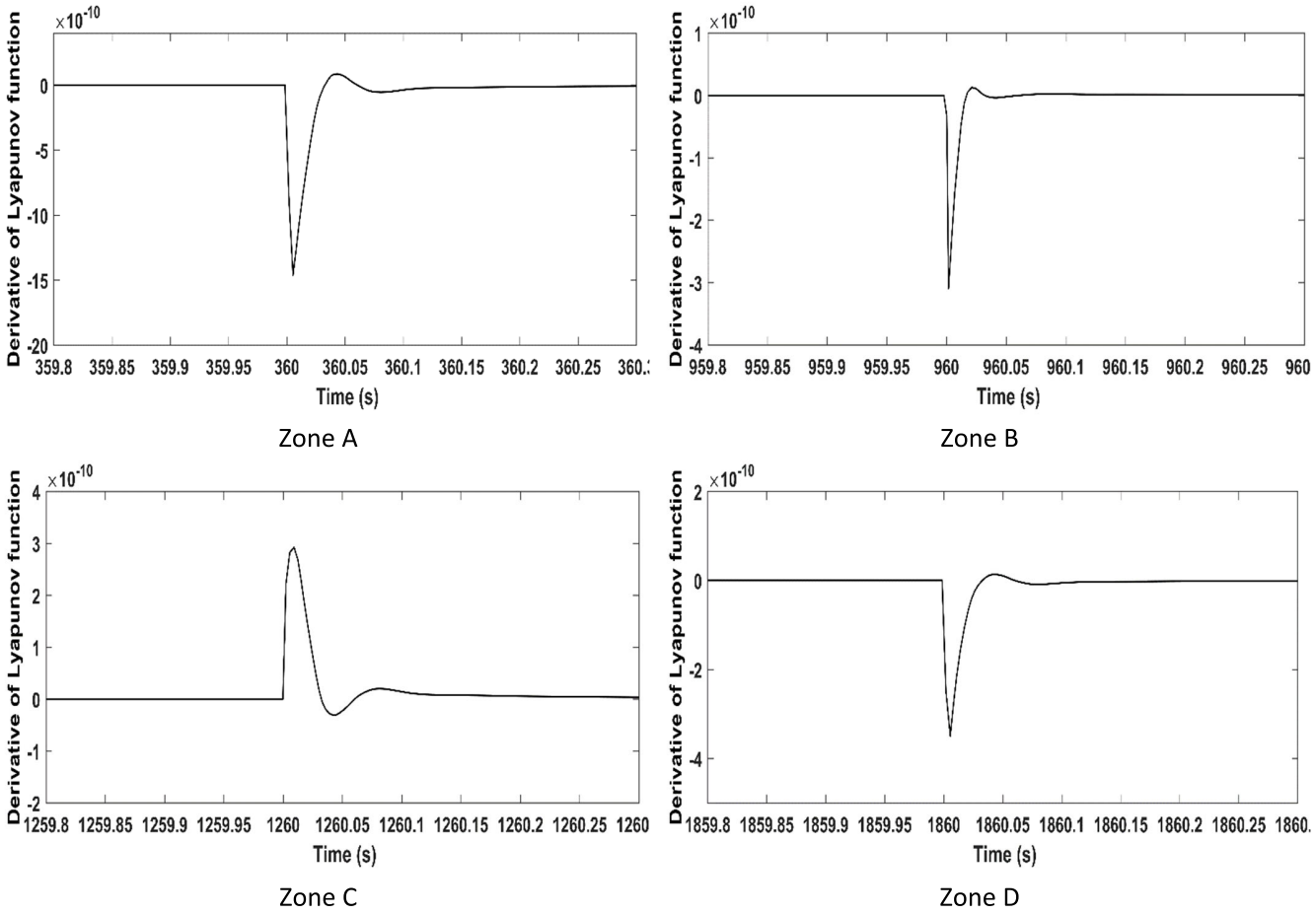

FIGURE 19. The derivative of the Lyapunov function with time for the FOPID controller in long time operation (case 2).

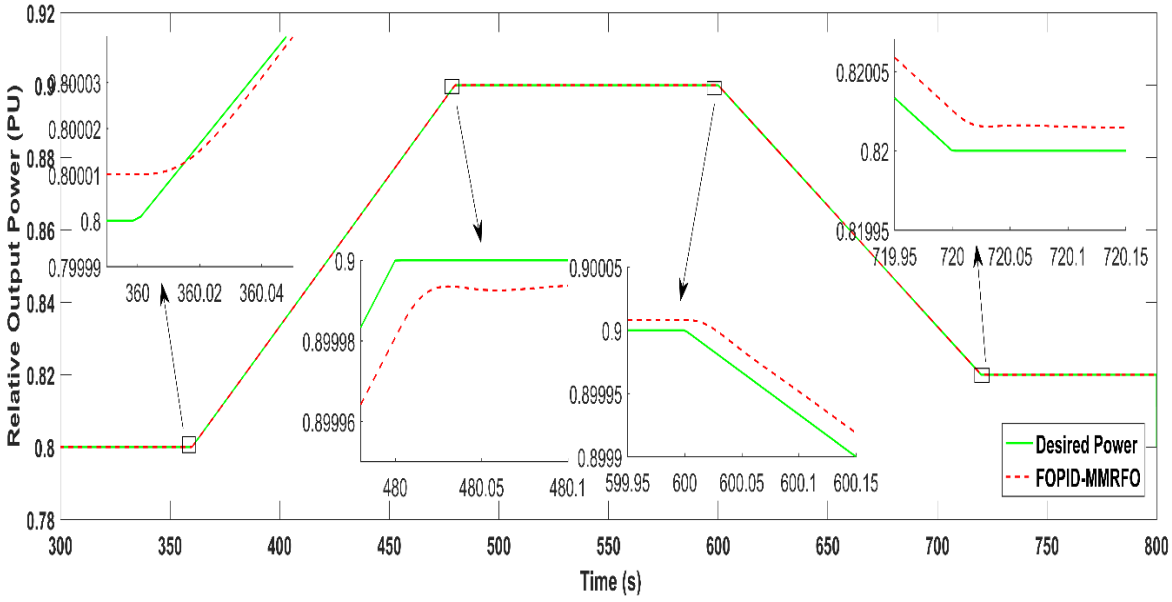

FIGURE 20. Output power in case 1 in the sensitivity analysis.

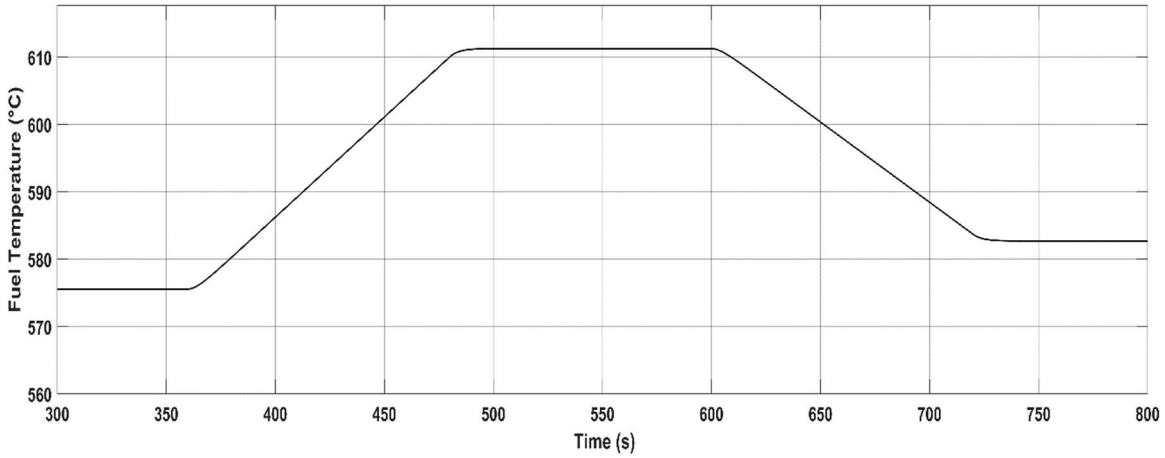

FIGURE 21. Fuel temperature in case 1 in the sensitivity analysis.

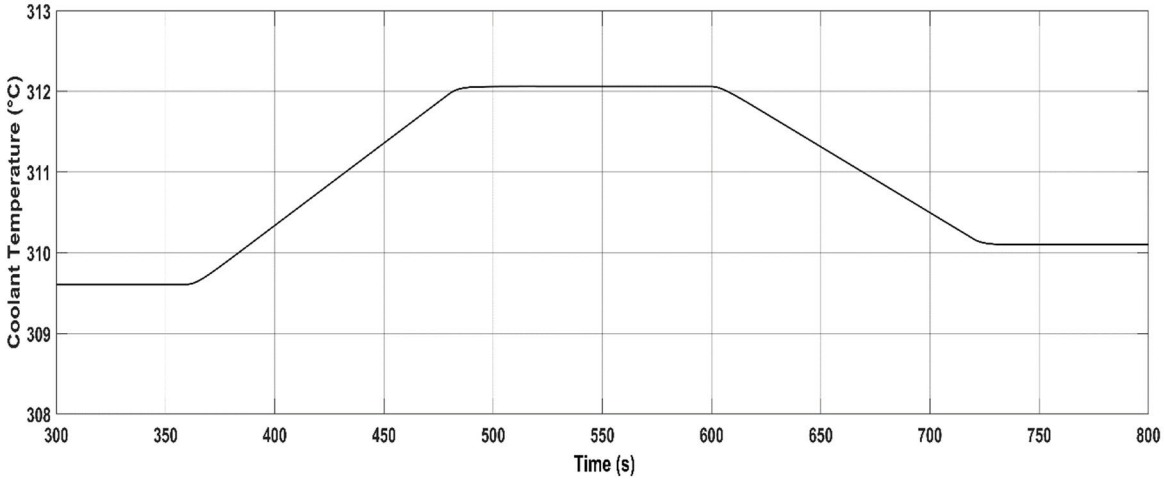

FIGURE 22. Coolant temperature in case 1 in the sensitivity analysis.

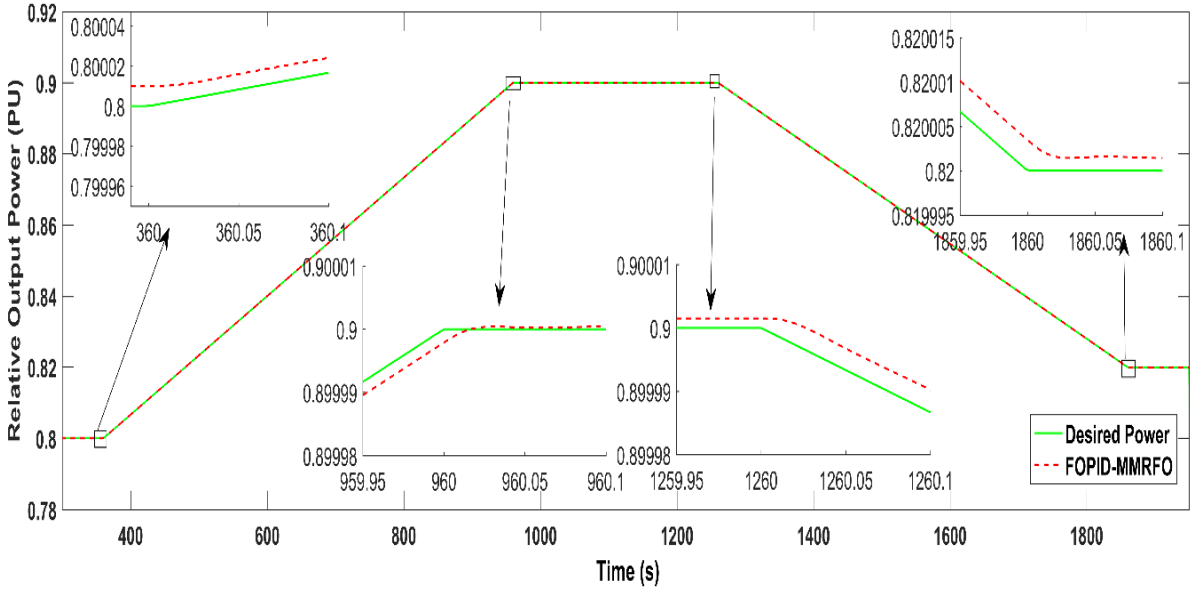

FIGURE 23. Output power in case 2 in the sensitivity analysis.

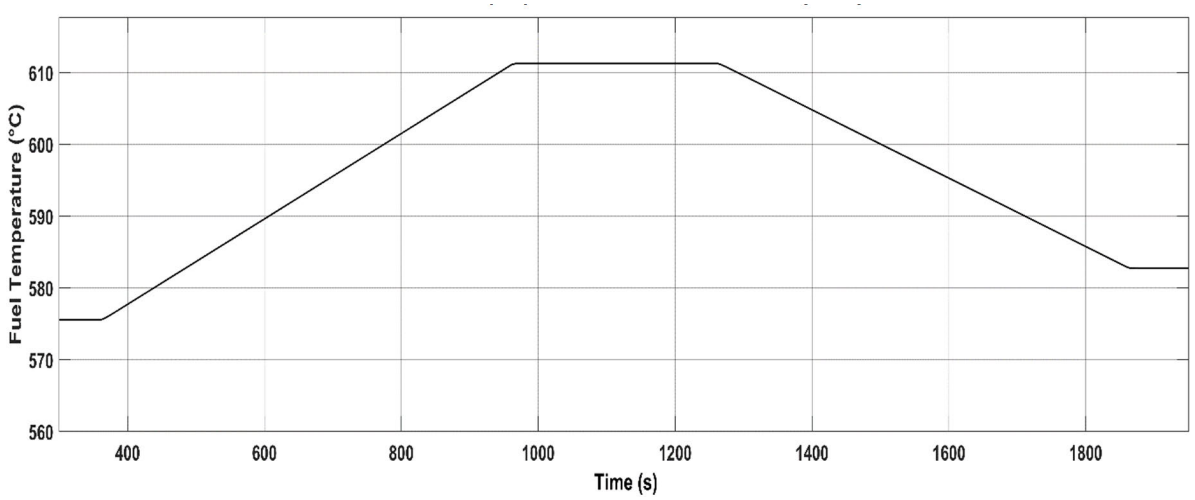

FIGURE 24. Fuel temperature in case 2 in the sensitivity analysis.

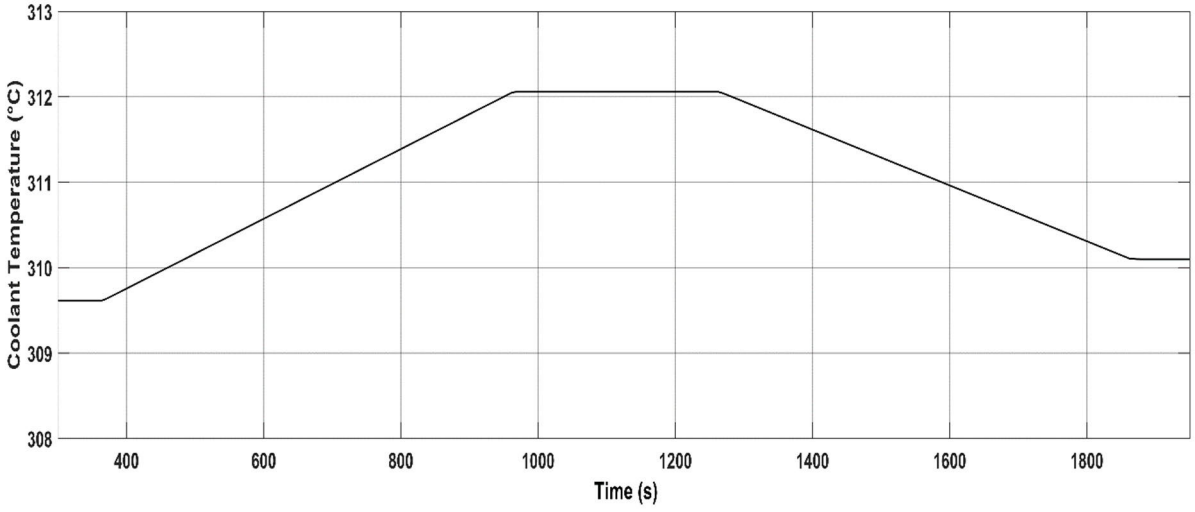

FIGURE 25. Coolant temperature in case 2 in the sensitivity analysis.

VI. CONCLUSION

In this paper, the operation of the PWRs in nuclear power plants is studied during load following operation instead of base load operation. A scheduled fractional order PID controller is designed to track the desired power output of a PWR during load following operation mode. A modified version of manta ray foraging optimization (MMRFO) algorithm is suggested to tune the controller parameters and the integral square error is considered to be the objective function. The proposed controller performance is tested and compared with the performance of a PID controller tuned by the MMRFO in both short and long duration operation of the PWR. The simulation results show that the FOPID controller has excellent accuracy in tracking the desired trajectory of the PWR output power with stable operation based on Lyapunov stability criterion. It is also noted that the control signal produced by the controller is accepted and will not cause any problem to control actuators that manage the operation of the reactor control rods as follows:

- For the short time operation the maximum overshoot (worst value) is $7.31 \times 10^{-3}\%$, maximum steady state error is 3.9×10^{-5} and maximum control rod speed is 0.095 cm/sec.
- For the long time operation the maximum overshoot is $1.3 \times 10^{-3}\%$, maximum steady state error (worst value) is 8.2×10^{-5} and maximum control rod speed is 0.019 cm/sec.

Also, to validate the proposed controller, a sensitivity analysis is performed which confirms the robustness of the controller. As a future recommendation, the authors suggest designing a scheduled FOPID controller or any other nonlinear controller

such as H-infinity controller to control the nuclear reactor output power in case of hard change in the desired output power. Also, the authors suggest taking into account both steam turbine and generator models to subsequently control the output electrical power of the plant.

REFERENCES

[1] O. Ozgur, V. Yilanci, and M. Kongkuah, "Nuclear energy consumption and CO_2 emissions in India: Evidence from Fourier ARDL bounds test approach," *Nucl. Eng. Technol.*, vol. 54, no. 5, pp. 1657–1663, May 2022, doi: 10.1016/j.net.2021.11.001.

[2] M. T. Majeed, I. Ozturk, I. Samreen, and T. Luni, "Evaluating the asymmetric effects of nuclear energy on carbon emissions in Pakistan," *Nucl. Eng. Technol.*, vol. 54, no. 5, pp. 1664–1673, May 2022, doi: 10.1016/j.net.2021.11.021.

[3] M. D. Mathew, "Nuclear energy: A pathway towards mitigation of global warming," *Prog. Nucl. Energy*, vol. 143, Jan. 2022, Art. no. 104080, doi: 10.1016/j.pnucene.2021.104080.

[4] Z. Dong, "Adaptive proportional-differential power-level control for pressurized water reactors," *IEEE Trans. Nucl. Sci.*, vol. 61, no. 2, pp. 912–920, Apr. 2014, doi: 10.1109/TNS.2014.2306208.

[5] V. Vajpayee, V. Becerra, N. Bausch, J. Deng, S. R. Shimjith, and A. J. Arul, "L_1-adaptive robust control design for a pressurized water-type nuclear power plant," *IEEE Trans. Nucl. Sci.*, vol. 68, no. 7, pp. 1381–1398, Jul. 2021, doi: 10.1109/TNS.2021.3090526.

[6] J. Hui, Y.-K. Lee, and J. Yuan, "Adaptive active fault-tolerant dynamic surface load following controller for a modular high-temperature gas-cooled reactor," *Appl. Thermal Eng.*, vol. 230, Jul. 2023, Art. no. 120727, doi: 10.1016/j.applthermaleng.2023.120727.

[7] H. Xia and X. Guo, "Modelling and coordinated control for load following of nuclear power plant," in *Proc. 41st Chin. Control Conf. (CCC)*, Jul. 2022, pp. 3527–3532, doi: 10.23919/ccc55666.2022.9902839.

[8] V. Vajpayee, V. Becerra, N. Bausch, J. Deng, S. R. Shimjith, and A. J. Arul, "Robust-optimal integrated control design technique for a pressurized water-type nuclear power plant," *Prog. Nucl. Energy*, vol. 131, Jan. 2021, Art. no. 103575, doi: 10.1016/j.pnucene.2020.103575.

[9] J. Hui, S. Ge, J. Ling, and J. Yuan, "Extended state observer-based adaptive dynamic sliding mode control for power level of nuclear power plant," *Ann. Nucl. Energy*, vol. 143, Aug. 2020, Art. no. 107417, doi: 10.1016/j.anucene.2020.107417.

[10] B. M. Patre, P. S. Londhe, and R. M. Nagarale, "Fuzzy sliding mode control for spatial control of large nuclear reactor," *IEEE Trans. Nucl. Sci.*, vol. 62, no. 5, pp. 2255–2265, Oct. 2015, doi: 10.1109/TNS.2015.2464677.

[11] L. Zhang, H. Xie, Q. Duan, C. Lu, J. Li, and Z. Lv, "Power level control of nuclear power plant based on asymptotical state observer under neutron sensor fault," *Sci. Technol. Nucl. Installations*, vol. 2021, pp. 1–8, Feb. 2021, doi: 10.1155/2021/8833729.

[12] J. Hui and J. Yuan, "Chattering-free higher order sliding mode controller with a high-gain observer for the load following of a pressurized water reactor," *Energy*, vol. 223, May 2021, Art. no. 120066, doi: 10.1016/j.energy.2021.120066.

[13] J. Hui, Y. Lee, and J. Yuan, "Fractional-order sliding mode load following control via disturbance observer for modular high-temperature gas-cooled reactor system with disturbances," *Asian J. Control*, vol. 25, no. 5, pp. 3513–3523, Sep. 2023, doi: 10.1002/asjc.3031.

[14] J. Hui and J. Yuan, "RBF-based adaptive sliding mode controller with extended state observer for load following of nuclear power plant," *Nucl. Eng. Design*, vol. 360, Apr. 2020, Art. no. 110465, doi: 10.1016/j.nucengdes.2019.110465.

[15] X. Liu, D. Jiang, and K. Y. Lee, "Decentralized fuzzy MPC on spatial power control of a large PHWR," *IEEE Trans. Nucl. Sci.*, vol. 63, no. 4, pp. 2343–2351, Aug. 2016, doi: 10.1109/TNS.2016.2580558.

[16] W. Zeng, Q. Jiang, Y. Liu, S. Yan, G. Zhang, T. Yu, and J. Xie, "Core power control of a space nuclear reactor based on a nonlinear model and fuzzy-PID controller," *Prog. Nucl. Energy*, vol. 132, Feb. 2021, Art. no. 103564, doi: 10.1016/j.pnucene.2020.103564.

[17] P. Wang, X. Yan, and F. Zhao, "Multi-objective optimization of control parameters for a pressurized water reactor pressurizer using a genetic algorithm," *Ann. Nucl. Energy*, vol. 124, pp. 9–20, Feb. 2019, doi: 10.1016/j.anucene.2018.09.026.

[18] M. Bhuyan, D. C. Das, A. K. Barik, and S. C. Sahoo, "Performance assessment of novel solar thermal-based dual hybrid microgrid system using CBOA optimized cascaded PI-TID controller," *IETE J. Res.*, vol. 68, pp. 1–18, Jun. 2022, doi: 10.1080/03772063.2022.2083026.

[19] S. M. H. Mousakazemi, "Comparison of the error-integral performance indexes in a GA-tuned PID controlling system of a PWR-type nuclear reactor point-kinetics model," *Prog. Nucl. Energy*, vol. 132, Feb. 2021, Art. no. 103604, doi: 10.1016/j.pnucene.2020.103604.

[20] S. M. H. Mousakazemi, N. Ayoobian, and G. R. Ansarifar, "Control of the reactor core power in PWR using optimized PID controller with the real-coded GA," *Ann. Nucl. Energy*, vol. 118, pp. 107–121, Aug. 2018, doi: 10.1016/j.anucene.2018.03.038.

[21] S. M. H. Mousakazemi, "Computational effort comparison of genetic algorithm and particle swarm optimization algorithms for the proportional–integral–derivative controller tuning of a pressurized water nuclear reactor," *Ann. Nucl. Energy*, vol. 136, Feb. 2020, Art. no. 107019, doi: 10.1016/j.anucene.2019.107019.

[22] S. M. H. Mousakazemi, N. Ayoobian, and G. R. Ansarifar, "Control of the pressurized water nuclear reactors power using optimized proportional-integral-derivative controller with particle swarm optimization algorithm," *Nucl. Eng. Technol.*, vol. 50, no. 6, pp. 877–885, Aug. 2018, doi: 10.1016/j.net.2018.04.016.

[23] B. Hekimoglu, "Optimal tuning of fractional order PID controller for DC motor speed control via chaotic atom search optimization algorithm," *IEEE Access*, vol. 7, pp. 38100–38114, 2019, doi: 10.1109/ACCESS.2019.2905961.

[24] M. Rafiei, G. R. Ansarifar, K. Hadad, and M. Mohammadi, "Load-following control of a nuclear reactor using optimized FOPID controller based on the two-point fractional neutron kinetics model considering reactivity feedback effects," *Prog. Nucl. Energy*, vol. 141, Nov. 2021, Art. no. 103936, doi: 10.1016/j.pnucene.2021.103936.

[25] D. Gupta, V. Goyal, and J. Kumar, "Design of fractional-order NPID controller for the NPK model of advanced nuclear reactor," *Prog. Nucl. Energy*, vol. 150, Aug. 2022, Art. no. 104319, doi: 10.1016/j.pnucene.2022.104319.

[26] O. Safarzadeh and O. Noori-kalkhoran, "A fractional PID controller based on fractional point kinetic model and particle swarm optimization for power regulation of SMART reactor," *Nucl. Eng. Des.*, vol. 377, Jun. 2021, Art. no. 111137, doi: 10.1016/j.nucengdes.2021.111137.

[27] M. Santhiya, A. Abraham, N. Pappa, and M. Chitra, "Reduced order model based optimally tuned fractional order PID controller for pressurized water nuclear reactor," *IFAC-PapersOnLine*, vol. 51, no. 4, pp. 669–674, 2018, doi: 10.1016/j.ifacol.2018.06.177.

[28] O. Karahan, "Design of optimal fractional order fuzzy PID controller based on cuckoo search algorithm for core power control in molten salt reactors," *Prog. Nucl. Energy*, vol. 139, Sep. 2021, Art. no. 103868, doi: 10.1016/j.pnucene.2021.103868.

[29] R. Lamba, S. K. Singla, and S. Sondhi, "Fractional order PID controller for power control in perturbed pressurized heavy water reactor," *Nucl. Eng. Des.*, vol. 323, pp. 84–94, Nov. 2017, doi: 10.1016/j.nucengdes.2017.08.013.

[30] J. Hui, Y.-K. Lee, and J. Yuan, "Load following control of a PWR with load-dependent parameters and perturbations via fixed-time fractional-order sliding mode and disturbance observer techniques," *Renew. Sustain. Energy Rev.*, vol. 184, Sep. 2023, Art. no. 113550, doi: 10.1016/j.rser.2023.113550.

[31] D. L. Hetrick. (1971). *Dynamics of Nuclear Reactors* [Online]. Available: https://www.osti.gov/biblio/4036735

[32] P. Ramaswamy, R. M. Edwards, and K. Y. Lee, "An automatic tuning method of a fuzzy logic controller for nuclear reactors," *IEEE Trans. Nucl. Sci.*, vol. 40, no. 4, pp. 1253–1262, Aug. 1993, doi: 10.1109/TNS.1993.8526778.

[33] H. Arab-Alibeik and S. Setayeshi, "Adaptive control of a PWR core power using neural networks," *Ann. Nucl. Energy*, vol. 32, no. 6, pp. 588–605, 2005, doi: 10.1016/j.anucene.2004.11.004.

[34] A. T. Mohamed, M. F. Mahmoud, R. A. Swief, L. A. Said, and A. G. Radwan, "Optimal fractional-order PI with DC–DC converter and PV system," *Ain Shams Eng. J.*, vol. 12, no. 2, pp. 1895–1906, Jun. 2021, doi: 10.1016/j.asej.2021.01.005.

[35] W. Zhao, Z. Zhang, and L. Wang, "Manta ray foraging optimization: An effective bio-inspired optimizer for engineering applications," *Eng. Appl. Artif. Intell.*, vol. 87, Jan. 2020, Art. no. 103300, doi: 10.1016/j.engappai.2019.103300.

[36] M. G. Hemeida, A. A. Ibrahim, A.-A.-A. Mohamed, S. Alkhalaf, and A. M. B. El-Dine, "Optimal allocation of distributed generators DG based manta ray foraging optimization algorithm (MRFO)," *Ain Shams Eng. J.*, vol. 12, no. 1, pp. 609–619, Mar. 2021, doi: 10.1016/j.asej.2020.07.009.
[37] M. Micev, M. Calasan, Z. M. Ali, H. M. Hasanien, and S. H. E. A. Aleem, "Optimal design of automatic voltage regulation controller using hybrid simulated annealing—Manta ray foraging optimization algorithm," *Ain Shams Eng. J.*, vol. 12, no. 1, pp. 641–657, Mar. 2021, doi: 10.1016/j.asej.2020.07.010.
[38] A. Tang, H. Zhou, T. Han, and L. Xie, "A modified manta ray foraging optimization for global optimization problems," *IEEE Access*, vol. 9, pp. 128702–128721, 2021, doi: 10.1109/ACCESS.2021.3113323.
[39] D. Simon, M. G. H. Omran, and M. Clerc, "Linearized biogeography-based optimization with re-initialization and local search," *Inf. Sci.*, vol. 267, pp. 140–157, May 2014.
[40] S. Mirjalili, S. M. Mirjalili, and A. Lewis, "Grey wolf optimizer," *Adv. Eng. Softw.*, vol. 69, pp. 46–61, Mar. 2014, doi: 10.1016/j.advengsoft.2013.12.007.
[41] S. Mirjalili and A. Lewis, "The whale optimization algorithm," *Adv. Eng. Softw.*, vol. 95, pp. 51–67, May 2016, doi: 10.1016/j.advengsoft.2016.01.008.
[42] W. Zhao, L. Wang, and Z. Zhang, "Atom search optimization and its application to solve a hydrogeologic parameter estimation problem," *Knowl.-Based Syst.*, vol. 163, pp. 283–304, Jan. 2019, doi: 10.1016/j.knosys.2018.08.030.
[43] P. N. Suganthan. (2005). *Problem Definitions and Evaluation Criteria for the CEC 2005 Special Session on Real-Parameter Optimization*. [Online]. Available: http://www.cs.colostate.edu/~genitor/functions.html
[44] Y. Wei, X. Zhao, Y. Wei, and Y. Chen, "Lyapunov stability criteria in terms of class K functions for Riemann–Liouville nabla fractional order systems," *ISA Trans.*, vol. 131, pp. 137–145, Dec. 2022, doi: 10.1016/j.isatra.2022.05.008.

TAREK A. BOGHDADY was born in Egypt, in March 1982. He received the M.Sc. and Ph.D. degrees in electrical power and machines engineering from Cairo University, Egypt, in 2011 and 2016, respectively. From 2005 to 2016, he was a Teaching Assistant with Cairo University, where he became an Assistant Professor in 2016 and an Associate Professor in 2022. His research interests include optimization, neural networks, FACTS, HVdc, utilization and generation of electric power, distributed generation, and renewable energy sources.

MOSTAFA MAHMOUD was born in Egypt, in May 1987. He received the B.S. and M.S. degrees in electrical power engineering from Cairo University, Egypt, in 2009 and 2015, respectively. His research interests include optimization, neural networks, modern control techniques, and sustainable energy generation and protection.

ESSAM ABOUL ZAHAB received the B.Sc. and M.Sc. degrees in electrical power and machines from Cairo University, Giza, Egypt, in 1970 and 1974, respectively, and the Ph.D. degree in electrical power from the University of Paul Sabatier, Toulouse, France, in 1979. He is currently a Professor with the Department of Electrical Power Engineering, Cairo University. His research interest includes sustainable energy generation and distribution.

ELSAYED TAG-ELDIN is currently with the Faculty of Engineering and Technology, Future University in Egypt, on leave from Cairo University after nearly 30 years of service with the Faculty of Engineering. He was the Dean of the Faculty of Engineering, Cairo University, where he achieved many unique signs of progress in both academia and research on the impact of emerging technologies in electrical engineering. He was a PI of several nationally and internationally funded projects. He has many publications in highly refereed international journals and specialized conferences on the applications of artificial intelligence in the protection of electrical power networks.

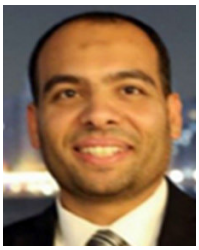

MAHMOUD SAYED was born in Cairo, Egypt, in 1982. He received the B.S., M.S., and Ph.D. degrees in electrical engineering from Cairo University, Egypt, in 2005, 2008, and 2013, respectively. He is currently an Assistant Professor with the Faculty of Engineering, Cairo University. His research interests include optimization and nuclear energy.